

**EFFECT OF SYNTHETIC STRUCTURAL FIBER
REINFORCEMENT ON THE FLEXURAL BEHAVIOR OF GFRP
REINFORCED CONCRETE BEAMS**

Atul Mani
CE13B17M100001

A Dissertation Submitted to
Indian Institute of Technology Hyderabad
In Partial Fulfilment of the Requirements for
The Degree of Master of Technology



भारतीय प्रौद्योगिकी संस्थान हैदराबाद
Indian Institute of Technology Hyderabad

Department of Civil Engineering

June 2018

Declaration

I declare that this written submission represents my ideas in my own words, and where others' ideas or words have been included, I have adequately cited and referenced the original sources. I also declare that I have adhered to all principles of academic honesty and integrity and have not misrepresented or fabricated or falsified any idea/data/fact/source in my submission. I understand that any violation of the above will be a cause for disciplinary action by the Institute and can also evoke penal action from the sources that have thus not been properly cited, or from whom proper permission has not been taken when needed.



(Signature)

Atul Mani

CE13B17M100001

Approval Sheet


This thesis entitled "Effect of Synthetic Structural Fiber Reinforcement on Flexural Behavior of GFRP Reinforced Beams" by Atul Mani is approved for the degree of Master of Technology from Indian Institute of Technology Hyderabad.



Prof. K.V.L. Subramaniam

Professor

Chairman



Dr. Anil Agarwal

Assistant Professor

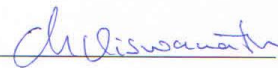
Examiner



Dr. S. Suriya Prakash

Associate Professor

Adviser



Dr. Viswanath Chinthapenta

Assistant Professor

External Examiner

Acknowledgements

I would like to express my deep sense of gratitude and sincere thanks to my advisor Dr. S. Suriya Prakash whose ideas helped me in doing my research work. His contribution to my research work is immense. It is all because of the time and effort he invested in me and my work, that I was able to finish this research work on time. He guided me through difficulties and helped me in achieving my objectives and setting a path for my career.

I would like to express my sincere gratitude towards Prof. K V L Subramaniam, Dr. A Rajagopal, Dr. Anil Agarwal, Dr. Surendra Nadh Somala and Dr. Mahendra Kumar Madhavan for providing me the required knowledge in my coursework which acted as a base to complete my thesis. I would like to extend my gratitude towards Dr. S. Surya Kumar for permitting me to carry out some part of my experimental work in the central workshop of IIT Hyderabad.

I would like to whole-heartedly thank Mr. M. Chellapandian (Research Scholar) for all his help and support during the experimental work, providing insights in doing the analysis and documentation of results. I would also like to thank Mr. Ganapathi Patil for his assistance during experimental work. Moreover, I would like to extend my thanks to our research group for their timely inputs to improve the quality of work. I would like to thank Mr. Gopal, Mr. Prashanth, Mr. Venkatesh and Mr. Raju for their assistance in carrying out experimental work. Their hard work and tireless effort to complete the experimental program is commendable.

Lastly, I would like to thank my family for whatever I am and will be. It is only because of them, their patience and sacrifices that I have been able to complete my post-graduation in a successful way.

Thank you very much.

Dedicated to

My family

Abstract

Corrosion of steel reinforcement is one of the major issues in reinforced concrete structures which affects its durability in the coastal environmental conditions. The use of fiber reinforced polymer (FRP) bars as an internal reinforcement has become prominent in the past decade to mitigate the problems associated with corrosion. However, the brittle failure mode of FRP reinforced beams is a major challenge for the design engineers and researchers. In this study, the use of structural synthetic fibers is proposed for improving the ductile behavior of RC beams with Glass Fiber Reinforced Polymer (GFRP) as internal reinforcement. Macro synthetic polyolefin fiber is chosen as the fiber reinforcing material. No previous work in past has focused on the use of macro synthetic polyolefin fibers in the performance improvement of GFRP bars reinforced concrete beams. Therefore, this study tries to fill in the knowledge gap existing in this research area and aims to provide experimental data for further development of analytical models and design equations. In total, ten reinforced beams were tested under flexure. The specimen includes: (i) control beam with steel reinforcement, (ii) GFRP reinforced beam without fibers, (iii) GFRP reinforced beams with 0.35%, 0.70%, and 1.00% synthetic fibers. To maintain the same stiffness across all the classes of specimens, in the beams reinforced with GFRP bars, the area of reinforcement is chosen to be equivalent to the area of steel used in control beam. The specimens were tested under four-point bending configuration in a displacement control mode. The experimental results are compared with the predictions obtained from the sectional analysis. Results were also compared from the data obtained from Digital Image Correlation (DIC) technique. Crack width is measured in constant moment zone with the help of DIC. Beams with GFRP reinforcement exhibited higher load carrying capacity (about 59%) but the ductility of the beam reduces significantly when compared to RC beams with steel reinforcement. Addition of fibers improved the ductility significantly when compared to GFRP reinforced beams without synthetic fibers. It is observed that the load carrying capacity for beams with 0.35%, 0.70%, and 1% fibers, increased by 72.6%, 100%, and 55% respectively when compared to beams with steel reinforcement. Moreover, at a higher fiber dosage of 1.0%, the peak strength is found to decrease though it had higher ductility and energy absorption.

Nomenclature

The following symbols are used in this thesis:

A_f	=	cross-sectional area of FRP bar;
A_s	=	cross-sectional area of steel bar;
E_f	=	modulus of elasticity of FRP bar;
E_s	=	modulus of elasticity of steel bar;

Carreira and Chu's equations:

E_{it}	=	initial tangent modulus;
f'_c	=	the compressive strength of concrete;
f_c	=	stress in plain concrete;
β	=	a material parameter that depends on the stress-strain diagram;
ε	=	strain in plain concrete;
ε'_c	=	strain corresponding to the compressive strength of plain concrete;

Chang et al.'s equations:

ε_{cf}	=	strain corresponding to the compressive strength of SFRC;
ε_{co}	=	strain at the peak stress of plain concrete;
\emptyset	=	diameter of the fiber;
f'_{cf}	=	compressive strength of SFRC;
RIv	=	reinforcing index;
V_f	=	fiber volume fraction;
ε_c	=	strain in steel fiber reinforced concrete;
σ_c	=	stress in steel fiber reinforced concrete;
l	=	length of the fiber;

ACI 440.1R-15 equations:

A_f	=	area of the tensile reinforcement;
b	=	width of the beam;
d	=	distance between extreme compression fiber and centroid of tensile reinforcement;
E_c	=	elastic modulus of plain concrete;
h	=	height of the beam;

I_{cr}	=	cracked moment of inertia;
I_e	=	effective moment of inertia;
I_g	=	gross moment of inertia;
L	=	length of the beam;
M_a	=	applied moment;
M_{cr}	=	cracking moment;
n_f	=	modulus ratio between FRP and plain concrete;
P	=	applied load;
S	=	shear span of the beam;
γ	=	factor related to loading and boundary conditions;
Δ	=	mid-span deflection;
ρ	=	reinforcement ratio;

H. Zhu et al.'s equations

x_0	=	depth of compression zone in gross section;
x_{cr}	=	depth of compression zone in cracked section;
A_{sf}	=	area of fibers in section;
n_{sf}	=	modulus ratio between fiber and plain concrete
ρ_{sf}	=	fiber volume fraction;

Table of Contents

Declaration	i
Approval Sheet	ii
Acknowledgements	iii
Abstract	v
Nomenclature	vi
List of tables	xi
List of figures	xii
Chapter 1 Introduction	1
1.1 General	1
1.2 Need for alternate reinforcement (FRP bars)	4
1.3 Use of fiber – reinforced concrete (FRC)	7
1.4 Concept of equivalent area	9
1.5 Digital Image Correlation (DIC)	11
1.6 Research motivation	13
1.7 Objectives and scope	14
1.8 Research methodology	14
Chapter 2 Literature Review	16
2.1 GFRP bars with fibers in flexure	16
2.2 FRP Bars Reinforced Concrete Beams under shear	21
2.3 Inferences from the Review of Literature	23
Chapter 3 Experimental Program	24
3.1 Specimen Preparation	24

3.2 Material Properties _____	26
3.2.1 Concrete _____	26
3.2.2 Macro-synthetic polyolefin fibers _____	27
3.2.3 Reinforcing Steel bars _____	28
3.2.4 Reinforcing GFRP bars _____	28
3.3 Test setup and instrumentation _____	30
3.3.1 Test setup _____	30
3.3.2 Instrumentation _____	31
Chapter 4 Test results and Discussions _____	33
4.1 General _____	33
4.2 Load- Deflection Behavior _____	33
4.2.1 Beams with steel as internal reinforcement without fibers (control specimens) _____	33
4.2.2 Beams with GFRP as internal reinforcement without fibers _____	35
4.2.3 Beams with GFRP as internal reinforcement with 0.35% fibers _____	35
4.2.4 Beams with GFRP as internal reinforcement with 0.70% fibers _____	36
4.2.5 Beams with GFRP as internal reinforcement with 1% fibers _____	36
4.2.6 Overall Comparison _____	36
4.3 Load – Strain _____	39
4.4 Failure mode comparison _____	41
4.5 Load-Displacement comparison (DIC & LVDT) _____	43
4.5 Crack width comparison _____	45
Chapter 5 Analytical Study _____	47
5.1 Analytical model for Moment-curvature predictions _____	47
5.1.1 General _____	47

5.1.2 Carreira and Chu model for plain concrete in compression _____	47
5.1.3 Chang et al. (2012) model for concrete with steel fibers in compression _____	48
5.1.4 Proposed model for concrete with macro-synthetic polyolefin fibers _____	48
5.1.5 Comparison of the test result and analytical predictions _____	49
5.2 Analytical model for load – deflection predictions _____	51
5.2.1 General _____	51
5.2.2. ACI 440.1R-15 model _____	51
5.2.3 Haitang Zhu et al. (2017) model _____	52
5.2.4 Comparison of test results with analytical predictions _____	53
Chapter 6 Summary and Conclusions _____	54
References _____	56

List of tables

<i>Table 1. 1: Mechanical properties of FRP bars</i>	6
<i>Table 3. 1: Test matrix</i>	25
<i>Table 3. 2: Results of cube and cylinder tests under compression</i>	26
<i>Table 3. 3: Details of mix design</i>	27
<i>Table 3. 4: Mechanical properties of Polyolefin fibers</i>	27
<i>Table 3. 5: Mechanical properties of Steel and GFRP bars</i>	28
<i>Table 4. 1: Summary of test results</i>	38
<i>Table 4. 2: Summary of Failure modes</i>	42
<i>Table 5. 1: Comparison of analytical and experimental results</i>	49
<i>Table 5. 2: Comparison of experimental and theoretical deflections at service load</i>	53

List of figures

<i>Figure 1. 1: Spalling of concrete due to corrosion</i> (www.ronacrete.co.uk)	1
<i>Figure 1. 2: Corrosion mechanism in steel</i> (Vavpetič, 2008)	2
<i>Figure 1. 3: Formation of corrosion products leading to spalling of concrete</i> (civildigital.com)	3
<i>Figure 1. 4: Materials used for combating corrosion</i> (www.materialsperformance.com)	4
<i>Figure 1. 5: (a) Soft Eye TBM (b) TBM drilling through shaft walls</i> (Dextra Group, 2017)	5
<i>Figure 1. 6: Types of FRP bars</i> (Source: www.zacarbon.com)	5
<i>Figure 1.7: Stress-strain plot of steel and GFRP bar</i>	7
<i>Figure 1. 8: Types of fibers</i> (fairmate.wordpress.com)	7
<i>Figure 1. 9: Behavior of steel fiber reinforced concrete</i>	8
<i>Figure 1. 10: Behavior macro-synthetic polyolefin FRC in tension and compression</i> (Aniket et. al, 2018)	9
<i>Figure 1. 11: Cross-sectional view of Beams with Steel and GFRP Equivalent Reinforcement</i>	10
<i>Figure 1. 12: Moment-curvature plot</i>	11
<i>Figure 1. 13: Schematic Diagram of the Deformation Relation</i>	11
<i>Figure 1. 14: DIC setup</i>	13
<i>Figure 1. 15: Methodology of work</i>	15
<i>Figure 2. 1: Beam specimen details</i> (Wang and Belarbi, 2010)	16
<i>Figure 2. 2: Moment curvature plot for beams with GFRP bars</i> (Wang and Belarbi, 2010)	17
<i>Figure 2. 3: Moment curvature plot for beams with CFRP bars</i> (Wang and Belarbi, 2010)	18
<i>Figure 2. 4: Load vs deflection for beams with different FRP reinforcement ratios</i> (Zhu et al., 2017)	19
<i>Figure 2. 5: Load vs deflection for beams with different FRHSC layer</i> (Zhu et al., 2017)	19
<i>Figure 2. 6: Beam specimen details</i> (Yang et al., 2012)	20
<i>Figure 2. 7: Load vs mid-span deflection for beams with different types of fibers</i> (Yang et al., 2012)	21
<i>Figure 2. 8: Beam specimen details</i> (Kaszubska et al., 2018)	22
<i>Figure 2. 9: Shear stress vs average mid-span deflection</i> (Kaszubska et al., 2018)	23
<i>Figure 3. 1: Beam specimen details</i> (dimensions in mm)	25
<i>Figure 3. 2: Tested cube and cylinder</i>	26
<i>Figure 3. 3: Distributing fibers in concrete mix</i>	27
<i>Figure 3. 4: Preparation of reinforcement cages with GFRP bars</i>	28

<i>Figure 3. 5: Test setup for tensile test (left) and GFRP bars after failure (right)</i>	29
<i>Figure 3. 6: Stress-strain curve for GFRP bars</i>	29
<i>Figure 3. 7: Schematic Representation of Test Setup</i>	30
<i>Figure 3. 8: Test setup and Instrumentation Details</i>	32
<i>Figure 4. 1: Load vs mid-span deflection for control beams</i>	34
<i>Figure 4. 2: Load vs mid-span deflection for beams with GFRP without fibers</i>	34
<i>Figure 4. 3: Load vs mid-span deflection for beams with GFRP with 0.35% fibers</i>	34
<i>Figure 4. 4: Load vs mid-span deflection for beams with GFRP with 0.70% fibers</i>	34
<i>Figure 4. 5: Load vs mid-span deflection for beams with GFRP with 1% fibers</i>	35
<i>Figure 4. 6: Overall load vs displacement comparison</i>	37
<i>Figure 4. 7: Load versus strain</i>	41
<i>Figure 4. 8: Failure Mode Comparisons for RC Beams</i>	43
<i>Figure 4. 9: Load-displacement comparison (DIC & LVDT)</i>	45
<i>Figure 4. 10: Load vs Crack width</i>	46
<i>Figure 4. 11: Contour of beams</i>	46
<i>Figure 5. 1: Moment-curvature comparison</i>	50

Chapter 1

Introduction

1.1 General

Steel is the most common reinforcement used in concrete elements to provide tensile strength and ductility. However, the corrosion of steel reinforcements in structural elements is a major issue for the buildings located in the coastal environmental conditions. Figure 1. 1 shows the spalling of concrete due to corrosion of steel reinforcement. Steel reinforcement embedded in concrete is typically protected from corrosion by a passive oxide layer that forms on the surface of the reinforcement. A passive layer is provided by the cement paste at high pH environment. However, if the oxide layer is broken down, in the presence of oxygen and moisture, corrosion can take place. At high chloride ion concentration, the corrosion is often initiated by chloride ions, which can penetrate the concrete to the level of the reinforcement and can lead to a breakdown of the protective oxide layer.



Figure 1. 1: **Spalling of concrete due to corrosion** (www.ronacrete.co.uk)

The corrosion of steel reinforcement in concrete is basically an electrochemical reaction. Concentration cells may be formed due to differences in concentration of dissolved ions near steel, such as alkalis, chlorides, and oxygen. This makes some parts of the metal anodic and the other cathodic (Figure 1. 2) which in turns creates a difference in electrical potential along the steel in concrete and an electrochemical cell is set up. These anodic and cathodic regions are connected by the electrolyte in the form of the pore water in the hardened cement paste. The positively charged ferrous ions Fe^{++} at the anode pass into solution while the negatively charged free electrons e^- pass through the steel into the cathode where they are absorbed by the constituents of the electrolyte and combine with water and oxygen to form hydroxyl ions $(OH)^-$. These travel through the electrolyte and combine with the ferrous ions to form ferric hydroxide which is converted by further oxidation to rust.

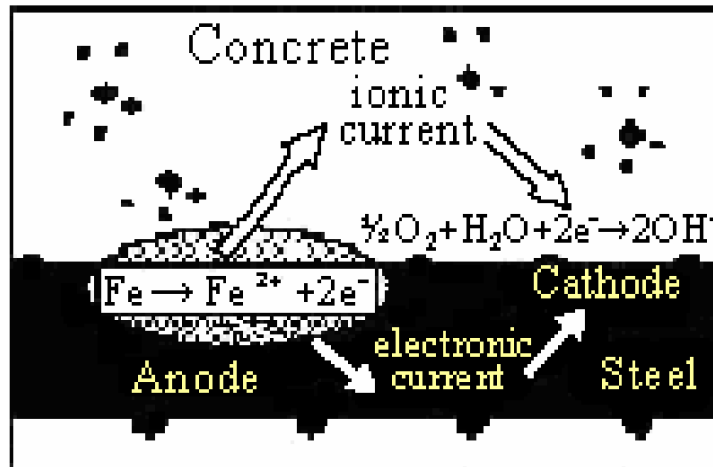
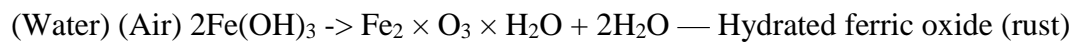
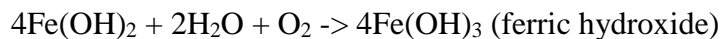
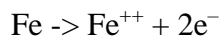
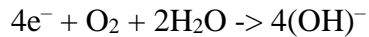


Figure 1. 2: Corrosion mechanism in steel (Vavpetič, 2008)

Anodic Reactions:



Cathodic Reactions:



The transformation of metallic iron to rust is accompanied by an increase in volume, which depending on the state of oxidation, may be as large as 600 percent of the original metal. This volume increase is the principal cause of concrete expansion and cracking. With the time corrosion products build up and cause more extensive cracking until the concrete breaks away from the bar eventually causing spalling. Figure 1. 3 shows the formation of corrosion product which eventually leads to spalling of concrete.

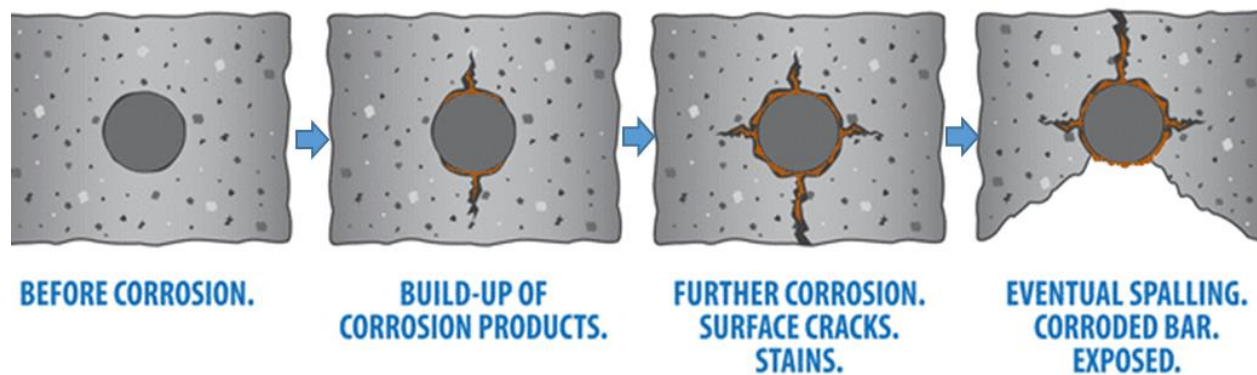
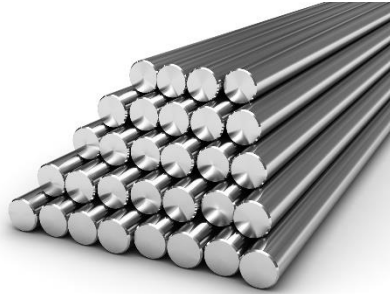


Figure 1. 3: **Formation of corrosion products leading to spalling of concrete** (civildigital.com)

Current methods of combating corrosion include protecting the reinforcing bar itself or decreasing the permeability of concrete to prevent ingress of chloride ions. Prominent technique for protecting the reinforcing bars is the application of epoxy coatings to the bars. Galvanized (Figure 1. 4 (a)) or stainless steel (Figure 1. 4 (b)) can be used as a replacement of steel. While, silica fumes (Figure 1. 4 (c)), fly ash and other pozzolans can be used to prevent the ingress of chloride ions. However, use of these methods is inhibited by cost and question of long-term effectiveness.



(a) Galvanized steel



(b) Stainless steel



(c) Silica fumes

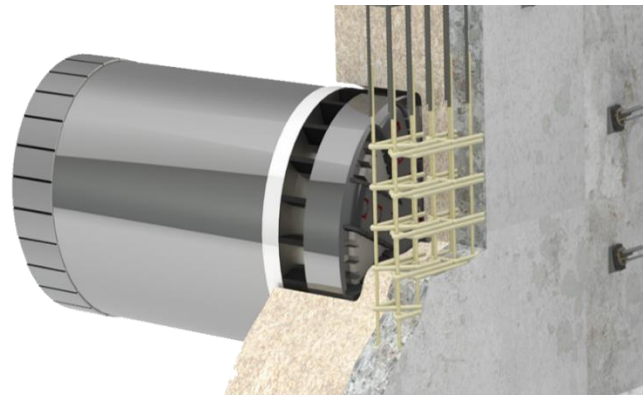
Figure 1. 4: **Materials used for combating corrosion** (www.materialsperformance.com)

1.2 Need for alternate reinforcement (FRP bars)

Recently, there has been a rapid increase in the use of fiber reinforced polymer (FRP) bars as a full or partial replacement for conventional steel reinforcements in reinforced concrete structures. FRP reinforcements possess high tensile strengths in comparison to the steel and, more importantly, it provides excellent resistant to corrosion. Additionally, FRP bars are non – magnetic in nature and are lightweight when compared to steel reinforcement. Due to these properties, use of FRP bars in structures located in coastal environmental conditions can improve the durability of concrete structures significantly. FRP can also find its application in hospital construction mainly because steel reinforcements can sometimes interfere with working of magnetic resonance imaging (MRI) machines. Replacing steel bars with the FRP bars, which posses non – magnetic behavior can eradicate such problems of magnetic interferences. FRP bars also finds its usage for tunneling purposes. FRP bars are used for building shaft walls (Figure 1. 5 (b)) which prevents the collapsing of overlaying surface. The soft eye tunnel boring machine (Figure 1. 5 (a)) has to drill through the walls. Steel reinforcement damages the blades of the boring machine while FRP bars made of fiber and resin does not damage the blades.



(a)



(b)

Figure 1. 5: (a) Soft Eye TBM (b) TBM drilling through shaft walls (Dextra Group, 2017)

FRP bars also have some characteristics that make them disadvantageous when compared to steel reinforcement. The elastic modulus of FRP bars are much less than that of steel bars. Glass fiber reinforced polymer (GFRP) bars have an elastic modulus of around 50 GPa, while the elastic modulus of Carbon fiber reinforced polymer (CFRP) bars have an elastic modulus between 120 to 150 GPa. Figure 1. 6 shows two types of FRP bars which are most common in use. Table 1. 1 shows the mechanical properties of different bars.



(a) CFRP bars



(b) GFRP bars

Figure 1. 6: Types of FRP bars (Source: www.zacarbon.com)

Table 1. 1: **Mechanical properties of FRP bars**

	Tensile strength (MPa)	Elastic Modulus (GPa)	Rupture strain (%)	Density (g/cm ³)
GFRP	480-1600	35-51	1.2-3.1	6.1-10.3
CFRP	600-3700	109-578	0.5-1.7	7.3-7.8
AFRP	1700-2500	41-125	1.9-4.4	6.1-6.9

The bond between concrete and FRP bars are also poor when compared to steel bars. A direct result of these characteristics is larger crack widths and larger deflections under service load. In addition, FRP materials display linear- elastic behavior in both tension and compression till failure and exhibit no yielding. Ductility is compromised and this makes it difficult to design members for a desired ductile failure mode. Figure 1.7 depicts the stress-strain plot of a typical steel and GFRP bar which clearly shows the linear stress-strain behavior of GFRP bar and its low stiffness when compared to steel.

To eradicate the disadvantages of FRP bars, new FRP bar and FRP reinforcement system were investigated. Hybrid FRP bars [Herris et al., (1998)] are one of the examples, which is fabricated with different continuous fibers. The stress-strain behavior of steel can be simulated by hybrid FRP bars. The ductility of hybrid FRP reinforced concrete beams was found to be close to the corresponding steel bar reinforced concrete beams. However, the complex fabrication process and high manufacturing cost of hybrid FRP bars have limited the engineering applications of hybrid FRP bars in concrete structures. A new reinforcement system consists of FRP and steel bars was also proposed [Qu et al. (2009)] which was found to improve the serviceability and ductility of FRP bar reinforced concrete beams. However, the corrosion of steel bars was not fully mitigated in this hybrid reinforcement system.

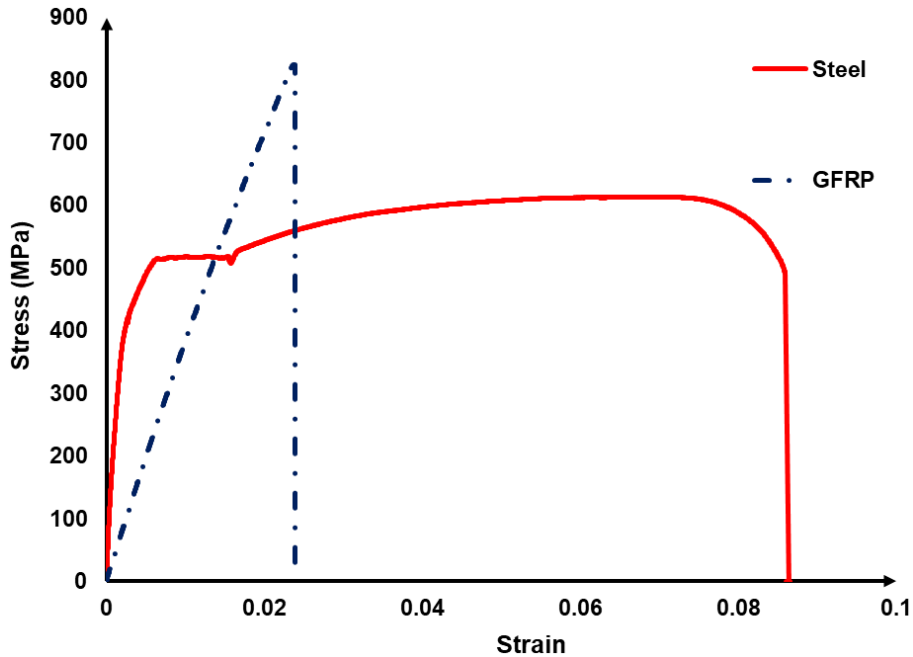


Figure 1.7: Stress-strain plot of steel and GFRP bar

1.3 Use of fiber – reinforced concrete (FRC)

To mitigate the problem of excessive crack width and reduction in ductility arising due to the use of FRP bars as internal reinforcement, fiber reinforced concrete (FRC) can be used in place of plain concrete, where discrete fibers act as secondary reinforcement. Figure 1. 8 shows different types of fibers used as secondary reinforcement in fiber reinforced concrete. Randomly distributed fibers in concrete mix can improve crack resistance in concrete. Usage of fibers improves post-peak behavior and post-cracking behavior of concrete under compression and tension respectively.



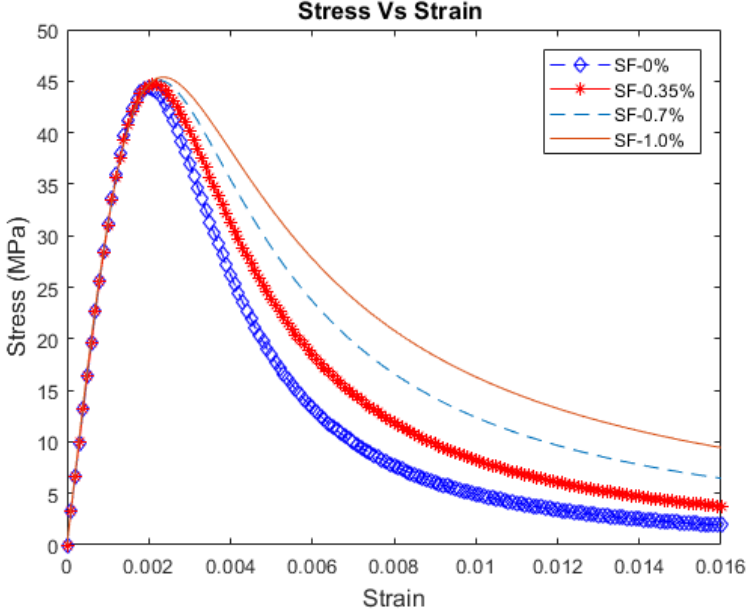
(a) Steel fibers

(b) Polyolefin fibers

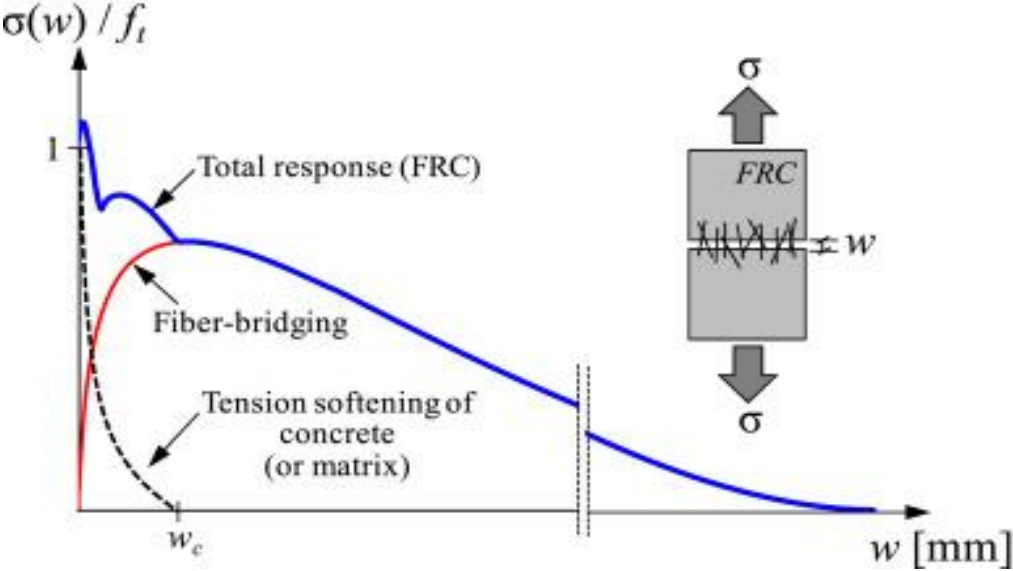
(c) Polypropylene fibers

Figure 1. 8: Types of fibers (fairmate.wordpress.com)

Figure 1. 9 shows the stress-strain behavior of steel fiber reinforced concrete in compression with different fiber dosage (a) and tension (b) while Figure 1. 10 shows the stress-strain behavior of macro-synthetic polyolefin fiber-reinforced concrete in tension and compression. FRC also improves toughness and avoids brittle shear failure and change it in ductile flexure failure.



(a) SFRC in compression



(b) SFRC in tension (Aniket et. al, 2018)

Figure 1. 9: Behavior of steel fiber reinforced concrete

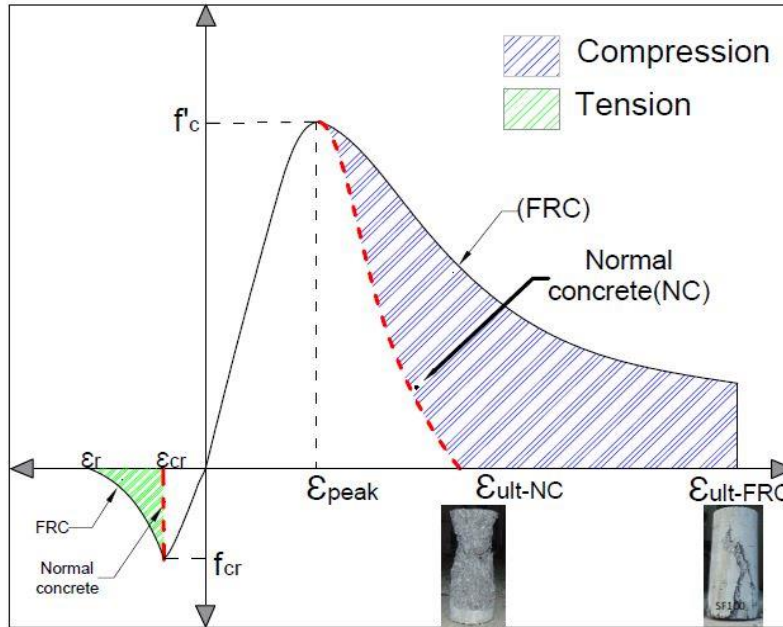


Figure 1. 10: Behavior macro-synthetic polyolefin FRC in tension and compression (Aniket et. al, 2018)

1.4 Concept of equivalent area

Post cracking stiffness of beams with GFRP bars are quite low when compared to beam with steel bars due to the low elastic modulus of GFRP bars. In order to attain the same stiffness for the beams with GFRP bars, the equivalent area of steel bar is taken for GFRP bars in the design of RC beams by keeping the product of area and elastic modulus is kept same for both the specimens.

$$A_s E_s = E_f A_f$$

Figure 1. 11 (a) & (b) shows the cross-sectional view of beam reinforced with steel and beam reinforced with the equivalent area (in tension zone only) of GFRP bar respectively. Modulus of elasticity of steel bar is around 200 GPa whereas modulus of elasticity of GFRP bar is around 50 GPa which is about 25% of steel.

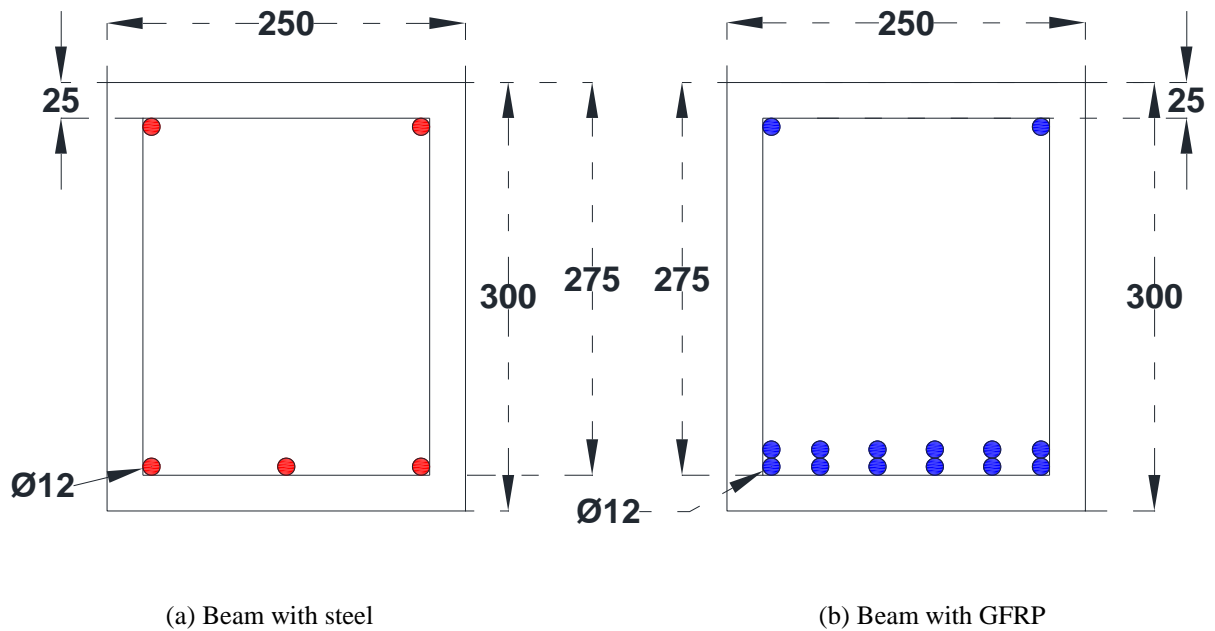
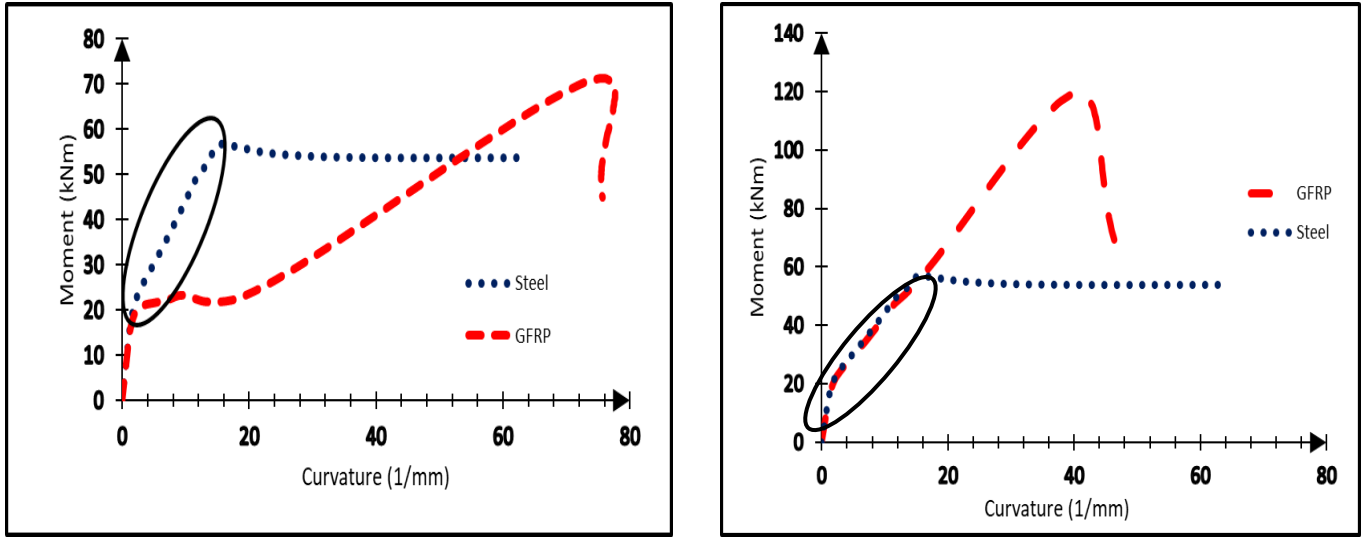


Figure 1. 11: **Cross-sectional view of Beams with Steel and GFRP Equivalent Reinforcement**

Figure 1. 12 (a) & (b) shows the moment-curvature plot of beam reinforced with steel and an equal area of GFRP bars and beam reinforced with steel and equivalent area of GFRP bars respectively. The model proposed by Chang et. al. (2012) is used for plotting the moment-curvature and is explained in section 5.3. In the Figure 1. 12 (a) one can see the reduction in stiffness of beam reinforced with GFRP bars after cracking whereas in Figure 1. 12 (b) where the equivalent area of GFRP bars is used, the stiffness is same as that of the beam reinforced with steel bars.



(a) Beam reinforced with steel and equal area of GFRP

(b) Beam reinforced with steel and equivalent area of GFRP

Figure 1.12: Moment-curvature plot

1.5 Digital Image Correlation (DIC)

DIC is an optical-based whole field surface displacement and strain measurement method. It is based on pattern matching between two images of the specimen coated by a random speckle pattern in the undeformed and deformed state. The specimen surface was initially coated with non-reflective white paint, and then black speckle was sprayed on the white coat. The basic principle of DIC method is to search for the maximum correlation between small zones (subsets) of the specimen image in the undeformed and deformed states, as illustrated in Figure 1.13.

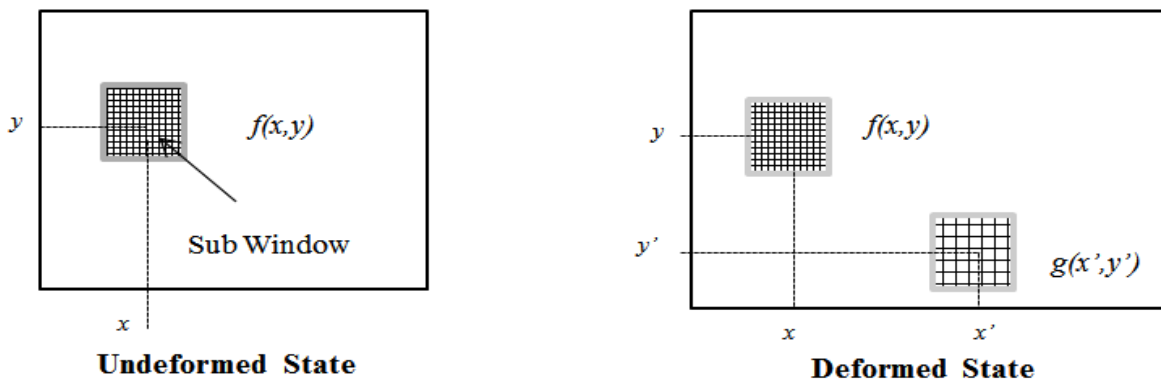


Figure 1.13: Schematic Diagram of the Deformation Relation

Based on the correlation between the subsets, the displacement field at different positions in the analysis region can be computed. The simplest image-matching procedure is the cross-correlation, which provides the in-plane displacement fields $u(x,y)$ and $v(x,y)$ by matching different zones of the two images. The cross-correlation coefficient is given in Eq. (a) and for correlation, small subregions over the digital image are compared.

$$C(u, v) = \frac{\sum_{i=0}^m \sum_{j=1}^m [f(x_i, y_i) - \bar{f}] [g(x'_i, y'_j) - \bar{g}]}{\sqrt{\sum_{i=1}^m \sum_{j=1}^m [f(x_i, y_i) - \bar{f}]^2} \sqrt{\sum_{i=1}^m \sum_{j=1}^m [g(x'_i, y'_j) - \bar{g}]^2}} \quad (\text{a})$$

where

$$x' = x + u_0 + \frac{\partial u}{\partial x} dx + \frac{\partial u}{\partial y} dy \quad (\text{b})$$

$$y' = y + v_0 + \frac{\partial v}{\partial x} dx + \frac{\partial v}{\partial y} dy \quad (\text{c})$$

where \bar{f} is mean intensity value of reference subset, \bar{g} is mean intensity value of deformed subset, m is the subset width in pixels, u_0 and v_0 are the translations of center of subsets along x and y direction respectively.

Images of the object's surface before and after deformation are recorded, digitized and stored in the computer. These images are then analyzed to determine the displacements by invoking a pattern matching principle. Since it is impossible to find matching points using single pixel, areas (called as subsets) containing multiple pixels are used for the analysis. The size of subset varies with respect to the experimentation details. The step size controls the density of analyzed data. For example, a step size of 5 will analyze every 5th point in each direction. A higher step size gives faster results but coarser data. A smaller step size will return more points but will take more computation time. For the present experiments, a subset size of 35 and a step size of five was chosen after a thorough sensitivity analysis. All the specimens had speckle pattern on the surface for capturing of DIC images. Two halogen lights were placed at an angle to the specimen to illuminate the specimen. The DIC camera was placed in front of the specimen with its axis normal to the specimen. Images were taken at regular intervals and were processed using specialized software (VIC- 2D) for strain analysis, crack initiation and propagation. The role of DIC is very

important in order to study the crack width and its propagation of crack in the beam and also the mid-span deflection. DIC technique has found profound application in various domains where the accuracy of strain measurements is a primary issue. However, the error in DIC measurement could arise due to many sources such as illumination variations, quality of acquisition system, camera lens distortion, image noise, or it could be due to the error associated with the implementation of correlation algorithms like subset size, step size, strain window size, sub-pixel optimization algorithm, and sub-pixel intensity interpolation scheme. Figure 1. 14 shows a typical DIC setup.

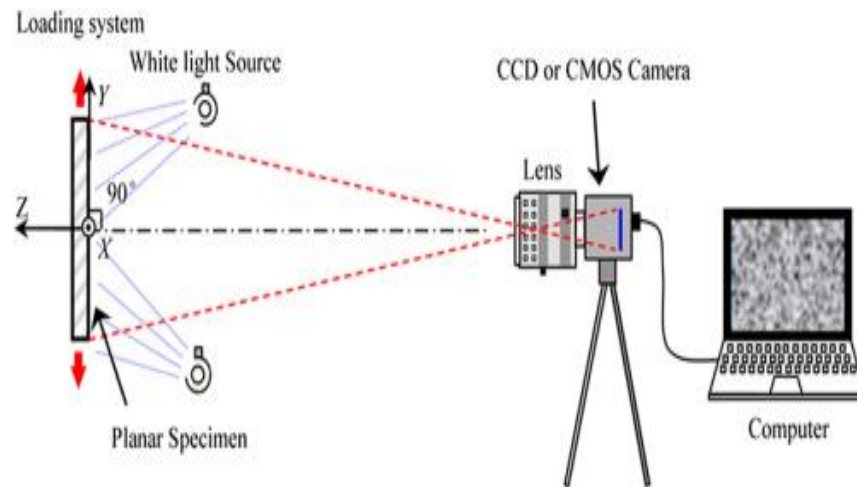


Figure 1. 14: DIC setup

1.6 Research motivation

The corrosion of steel bars can drastically reduce the capacity of a structure. Replacing steel bars with GFRP bars can mitigate the problem of corrosion but ductility of the beam is also lost on the other hand. With the addition of macro-synthetic fibers in concrete, the ductility behavior of a FRP reinforced concrete beams can be improved. Use of structural macro-synthetic fibers has not been explored in past for improving the ductility of GFRP bars reinforced concrete beams. Macro-synthetic polyolefin fibers can arrest the structural cracks as well without increasing the overall cost of the project.

1.7 Objectives and scope

The use of fiber reinforced concrete with FRP bars is one of the possible ways to replace conventional steel reinforcement. In this study, GFRP bar is used as it is economical when compared to CFRP bar and is readily available. In addition, macro-synthetic fibers are used as secondary reinforcement. The main objective of this study is to investigate the flexural behavior of reinforced concrete beams with GFRP bars as longitudinal reinforcement. To study the behavior of macro synthetic polyolefin fibers on the overall performance enhancement of GFRP reinforced concrete beams under flexure is also one of the main objectives of this study. Also, crack width model for fiber reinforced concrete beams reinforced with GFRP bars will be developed.

The scope of the work is as follows:

- To conduct a full-scale experimental study on the behavior of GFRP reinforced RC beams.
- To carry out analytical investigation by developing an improved constitutive relation for synthetic fiber reinforced concrete
- To develop a non-linear 3-D finite element model for GFRP reinforced beams with and without fibers and carry out an extensive parametric investigation.

1.8 Research methodology

The methodology of the work will incorporate the testing of full-scale RC beams to investigate the influence of several parameters like FRP reinforcement ratio, the aspect ratio of fibers and failure mode under flexure. The proposed work methodology is depicted in Figure 1. 15.

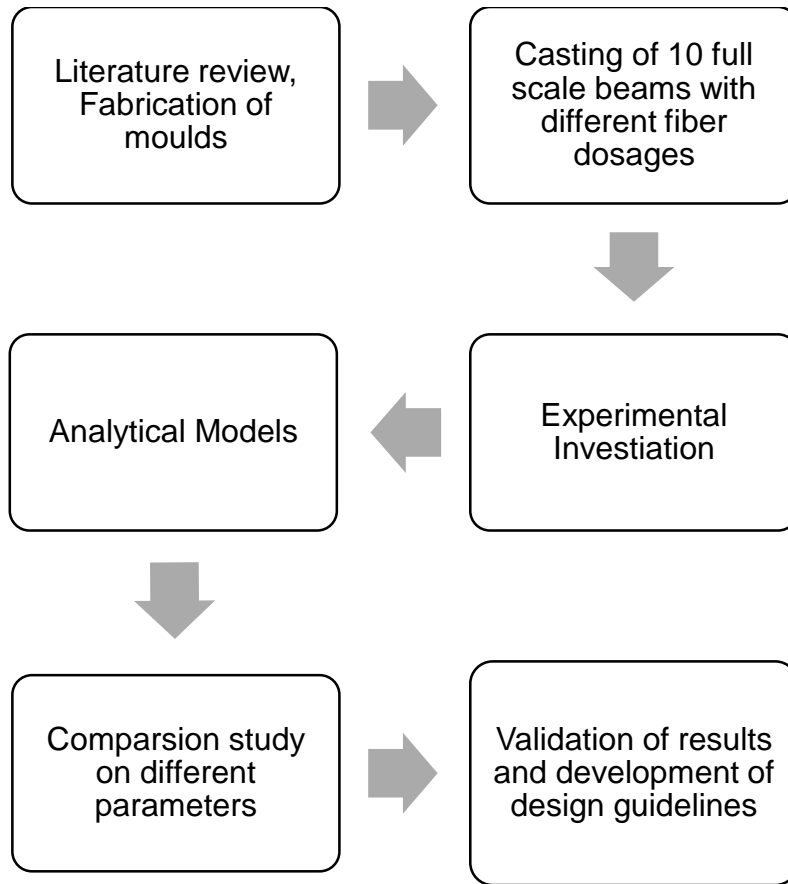


Figure 1. 15: **Methodology of work**

Chapter 2

Literature Review

Usage of FRP bars with fiber reinforced concrete is one of the best alternatives for steel bars. For the last few decades, numerous researchers are working on the usage of FRP as longitudinal reinforcement in FRC and to develop ductile FRP reinforced FRC.

2.1 GFRP bars with fibers in flexure

Wang and Belarbi (2011) in their work, investigated the ductility and crack width behavior of 12 reinforced concrete beams under flexure by varying FRP rebar size, FRP type (CFRP/GFRP) and concrete type (plain/FRC). They used polypropylene fiber with a fixed fiber volume fraction of 0.5% to ensure good workability of concrete. Beams were over reinforced and were designed to fail by concrete crushing. Figure 2. 1 shows the beam specimen details for the experiment carried out by Belarbi and Wang.

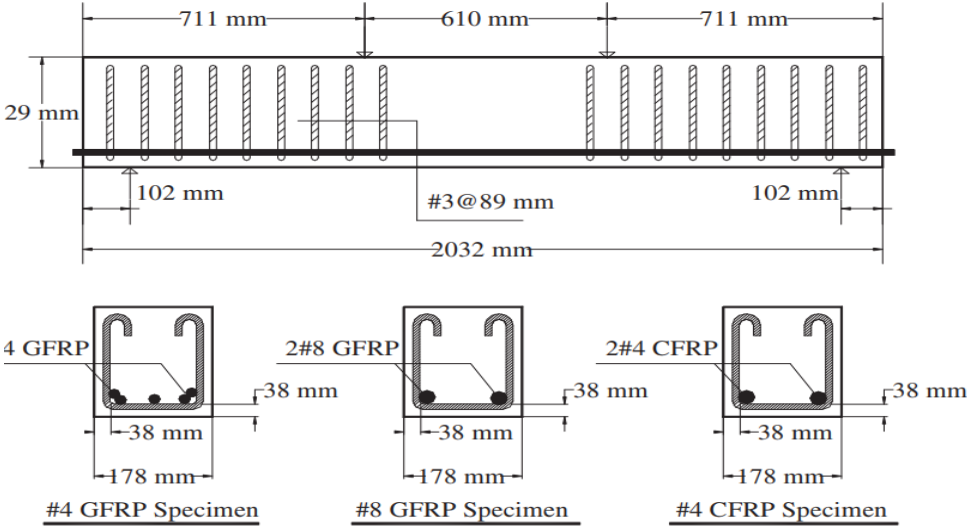


Figure 2. 1: Beam specimen details (Wang and Belarbi, 2010)

The specimens were tested under four-point bending configuration. LVDTs and strain gauges were deployed to measure the mid-span deflection, curvature, and strain in the beams. The important

findings from their work are that the crack width decreased with the addition of fibers. Moreover, the ductility of the beams increased by more than 30% in comparison to the control beam without fibers. Figure 2. 2 shows the moment-curvature plot for beams with and without fiber in the concrete mix. Both the beams have GFRP as internal reinforcement. The plot with P4G as label is for beam with plain concrete and GFRP as internal reinforcement while the plot with F4G label is for beam with fiber reinforced concrete and GFRP as internal reinforcement.

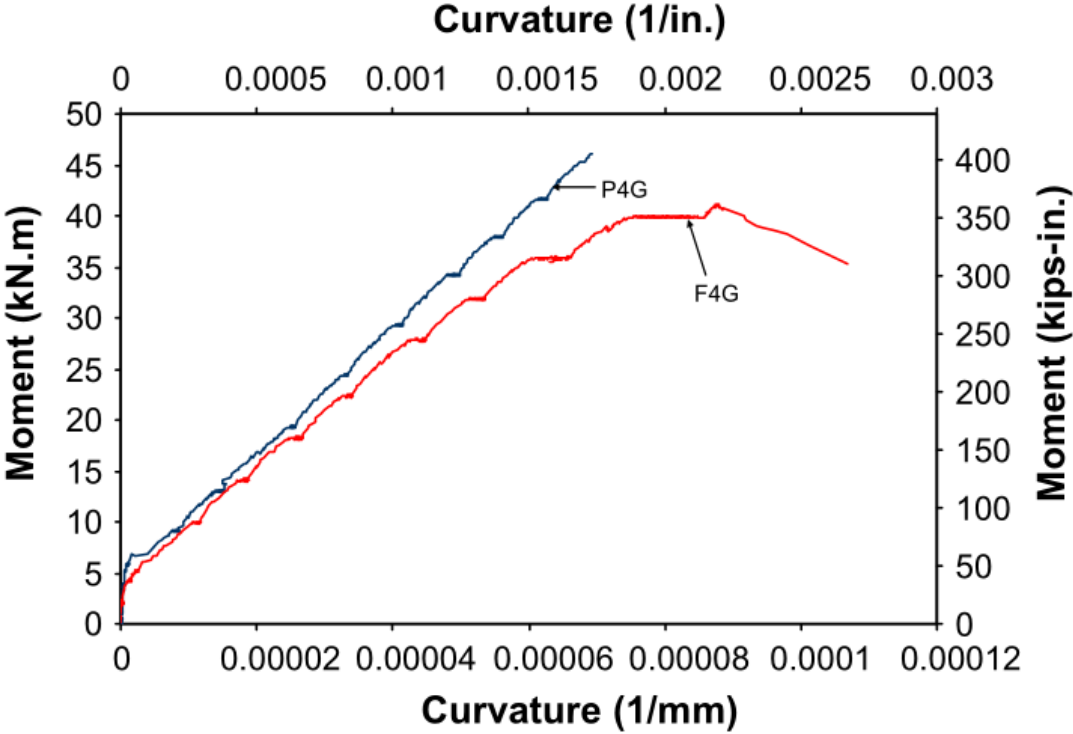


Figure 2. 2: Moment curvature plot for beams with GFRP bars (Wang and Belarbi, 2010)

Similarly, Figure 2. 3 shows the moment-curvature plot for beams with and without fiber in the concrete mix. Both the beams have CFRP as internal reinforcement. The plot with P4C as label is for beam with plain concrete and CFRP as internal reinforcement while the plot with F4C label is for beam with fiber reinforced concrete and CFRP as internal reinforcement.

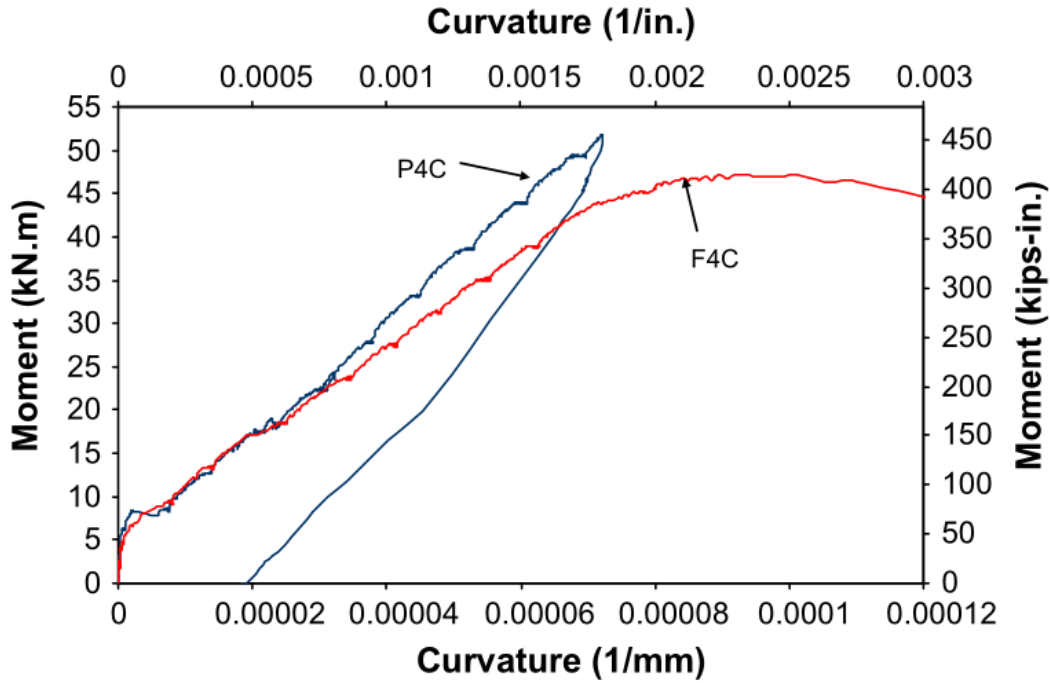


Figure 2. 3: **Moment curvature plot for beams with CFRP bars (Wang and Belarbi, 2010)**

Zhu et al. (2017) in his work investigated the flexural behavior of partially FRHSC beams reinforced with FRP (Basalt) bars including flexural capacity, deflection and cracking response and ductility. Hooked steel fibers and high strength concrete (HSC) were used in the experiment. The thickness of FRHSC layer, steel fiber volume fraction and FRP reinforcement ratios were varied. Results from his work concluded that increasing the FRP reinforcement ratio is an effective way to improve the flexural capacity of partially FRHSC beams reinforced with FRP bars. Figure 2. 4 shows the load vs deflection plot of beams with different reinforcement ratio. The specimen with label B2P1-3, B2P2-3, B2P3-3 & B2P4-3 has reinforcement ratio as 0.50%, 0.68%, 1.03% and 1.37% respectively. The effects of thickness of FRHSC layer and fiber volume fraction on the flexural capacity were not highly significant. However, for fully FRHSC beams reinforced with FRP bars, the flexural capacity was significantly greater than that of partially FRHSC beams. Also, the failure mode changed from concrete crushing to FRP bar rupture in fully FRHSC beams. Increasing the thickness of FRHSC layer, steel fiber volume fraction and FRP reinforcement ratio resulted in proportional decrease in the deflection, crack width and crack deviation. But the

ductility of partially FRHSC beams reinforced with FRP bars reduced with the increase of the thickness of FRHSC layer and steel fiber volume fraction. Figure 2. 5 shows the load vs deflection plot of beams with different FRHSC layer. The specimen with label B2A0, B2P2-1, B2P2-2, B2P2-3 & B2A2 has thickness of FRHSC layer as 0 mm, 90 mm, 130 mm, 170 mm and 300 mm respectively. It can be clearly seen that the ductility is decreasing as the thickness of FRHSC layer is increased from 0 to 170 mm. But the ductility increased when the steel fibers are added to the full depth of the beam i.e., 300mm.

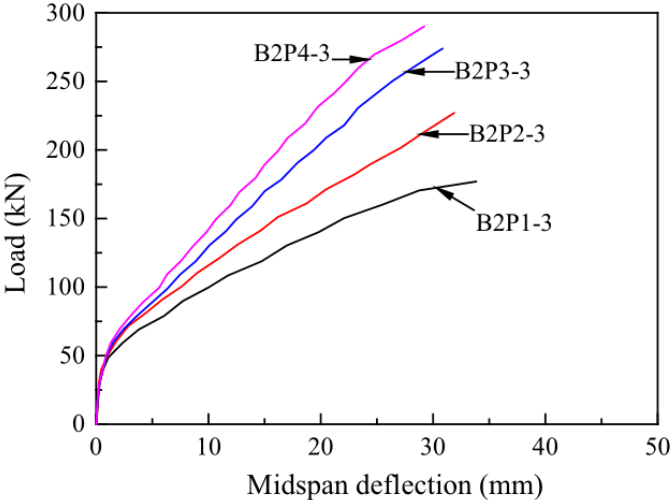


Figure 2. 4: Load vs deflection for beams with different FRP reinforcement ratios (Zhu et al., 2017)

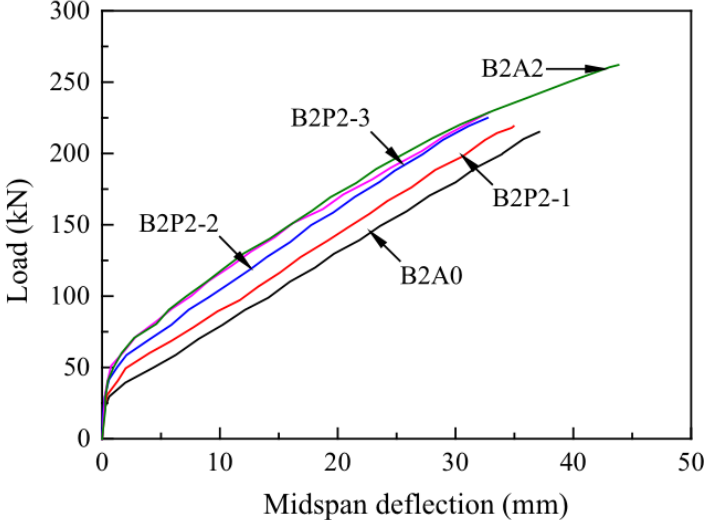
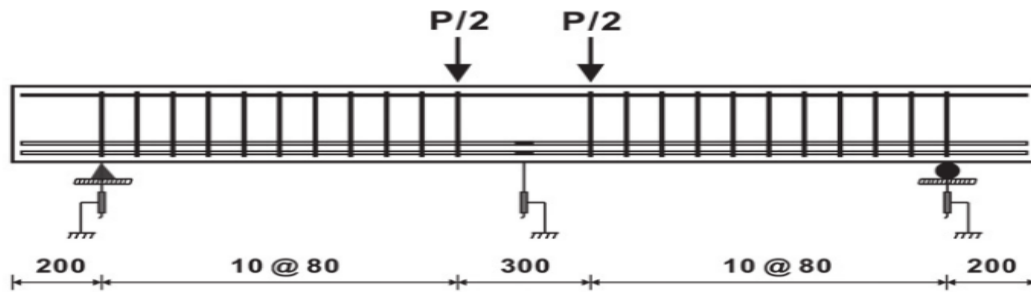


Figure 2. 5: Load vs deflection for beams with different FRHSC layer (Zhu et al., 2017)

Yang et al (2012) in his work investigated the influence of addition of fiber on load carrying capacity, cracking response and ductility of high strength concrete beams with FRP bars. The beams consisted of two different types of FRP bars namely CFRP and GFRP and also two different types of fibers namely hooked steel fibers and crimped polyolefin synthetic fibers. The fiber volume fraction was kept constant, 2% for polyolefin fibers and 1% for steel fibers. In order to provide similar nominal flexural strength for the beams with GFRP and CFRP bars, six 13 mm GFRP bars and four 9 mm CFRP bars were used.



(a) Reinforcement details and location of strain gauges and LVDTs



(b) Section details of beam with GFRP bars (left) and CFRP bars (right)

Figure 2. 6: Beam specimen details (Yang et al., 2012)

Major conclusions drawn from the experiments were, the addition of fibers delayed the initiation of flexural cracks and decreased the crack widths. Ductility of GFRP bar with steel and synthetic fibers increased by 70% and 80% respectively, while no improvement of ductility was observed by addition of fibers in case of CFRP. Figure 2. 7 (a) & (b) shows the load vs mid-span deflection of beams with GFRP bars without fibers (GG), with steel fibers (GG-ST), with synthetic fibers

(GG-SN) and beams with CFRP bars without fibers (CC), with steel fibers (CC-ST), with synthetic fibers (CC-SN) respectively.

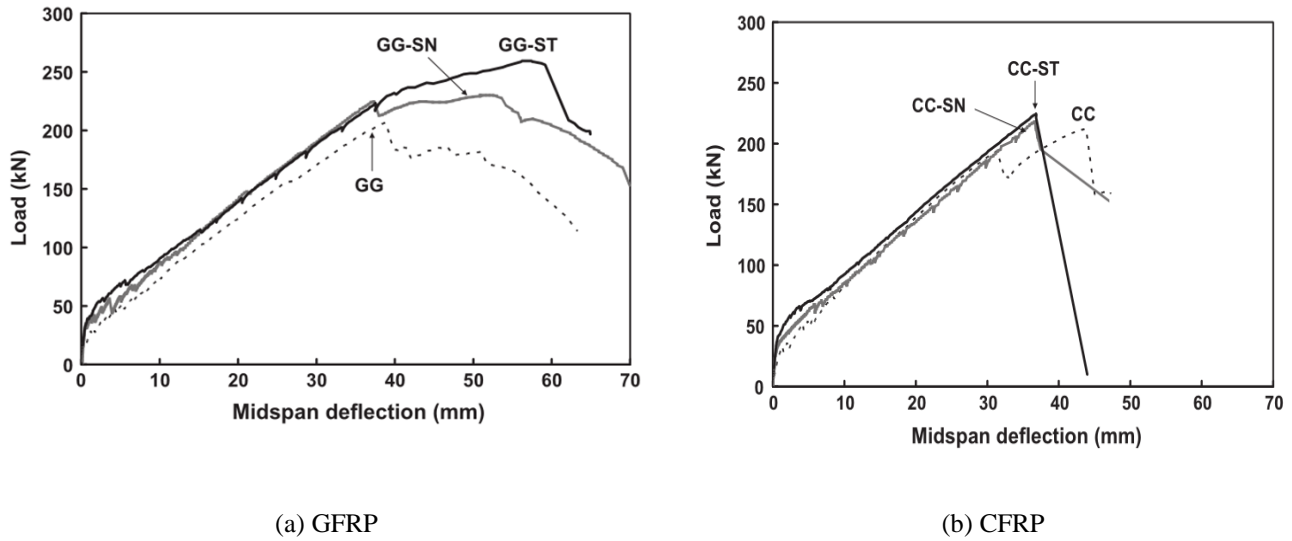


Figure 2. 7: Load vs mid-span deflection for beams with different types of fibers (Yang et al., 2012)

2.2 FRP Bars Reinforced Concrete Beams under shear

Kaszubska et al. (2018), investigated the shear behavior of GFRP bars reinforced concrete beams. Seven T-shaped beams were cast with varying reinforcement ratio (1%, 1.4%, and 1.8%) and tested. The authors used digital image correlation technique to observed the behavior. The bars were arranged in different number of layers and different number of bars in each layer and their influence on the shear behavior of the beam is also studied in her work. Figure 2. 8 shows the specimen details of the beams.

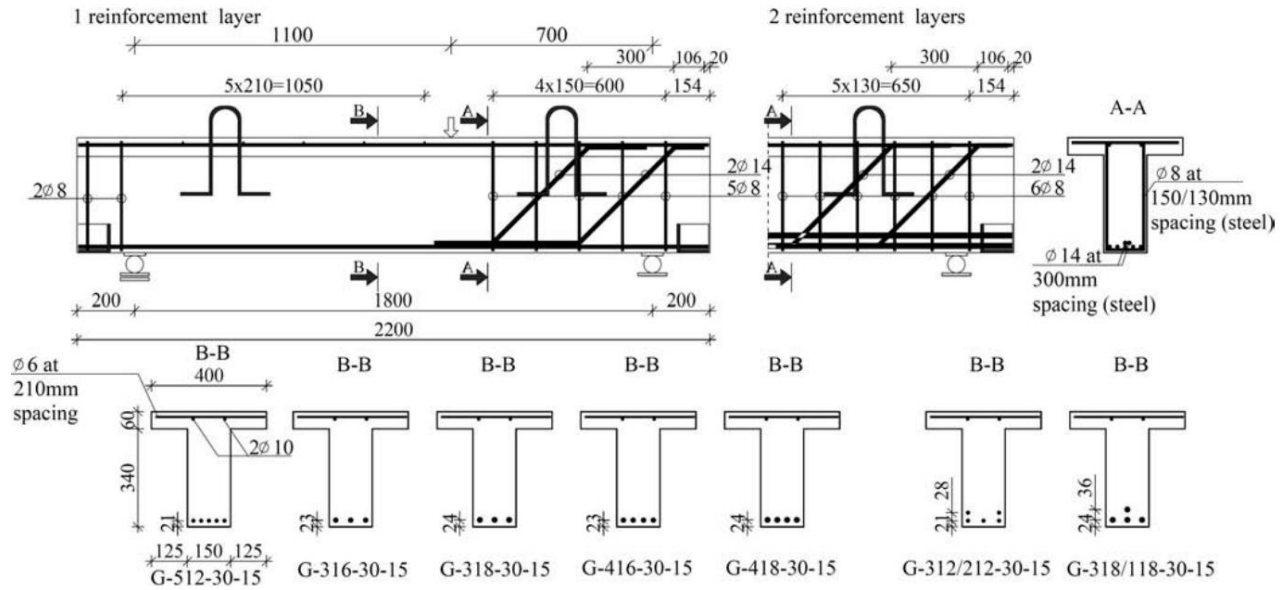


Figure 2. 8: **Beam specimen details (Kazubaska et al., 2018)**

The authors concluded that the shear failure crack has a tendency to increase with the flexural reinforcement ratio. With the increase in the flexural reinforcement ratio, the beam's loading carrying capacity and the stiffness have increased due to the decrease of the maximum crack opening. Higher FRP ratio had favorable effects on the concrete aggregate interlock and dowel shear stress mechanisms. Placing the flexural bars in two layers increases the shear strength by 28% when compared to the beam with same reinforcement ratio, but placed in one layer. Doubling the reinforcement ratio caused an increase in the beam's shear capacity of 11% when the flexural reinforcement was disposed of in one layer. However, it increased to 25% when arranged in two layers. Figure 2. 9 shows the shear stress versus mid-span deflection of different beams.

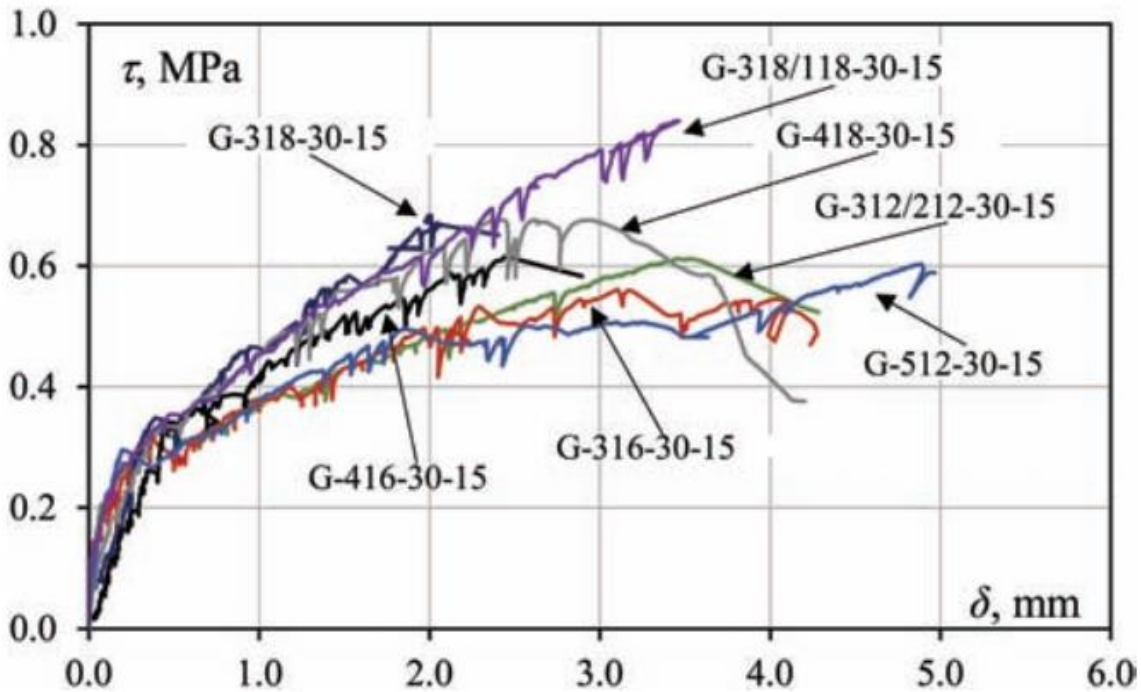


Figure 2. 9: Shear stress vs average mid-span deflection (Kaszubska et al., 2018)

2.3 Inferences from the Review of Literature

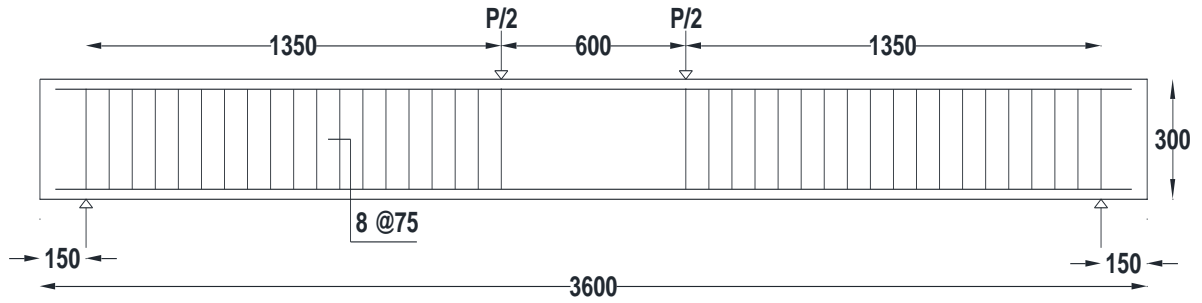
- Beams with FRP bars have higher load carrying capacity than the corresponding beams with an equal area of steel bars.
- Load carrying capacity increased with increase in FRP reinforcement ratio.
- Beams with FRP bars failed typically in a brittle mode.
- Fiber reinforced concrete can increase the ductility of the beams with FRP bars.
- Crack widths reduced in case of fiber reinforced concrete when compared with plain concrete GFPR reinforced beams.
- Addition of fibers delayed the initiation of the cracks and provided pseudo-ductility.
- Increasing the flexural reinforcement ratio increased the shear capacity of the FRP reinforced beams.

Chapter 3

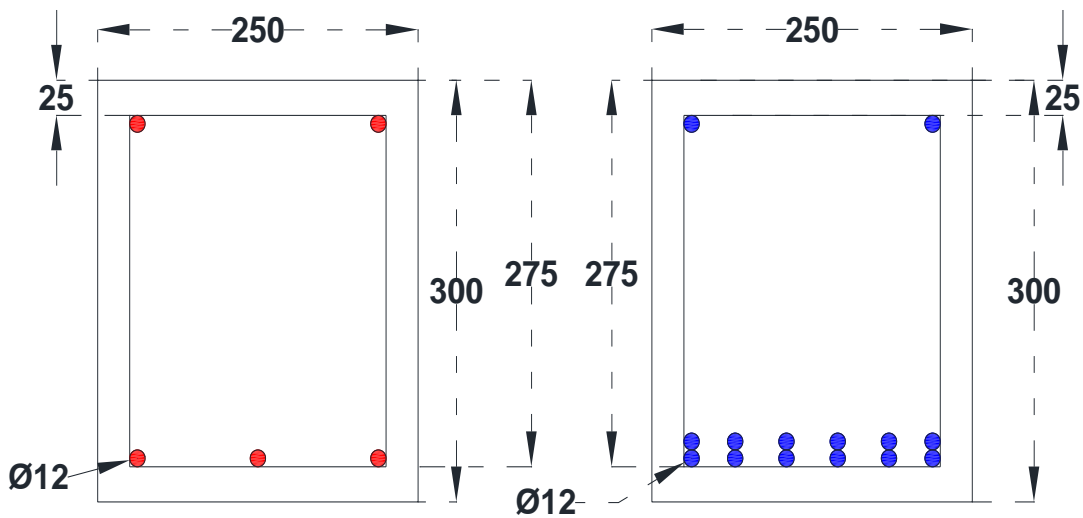
Experimental Program

3.1 Specimen Preparation

In total, ten reinforced concrete beams were cast which includes two control beams with steel reinforcement, two beams with GFRP bars without fibers (control specimens) and six beams with GFRP bars and varying fiber dosages (0.35%, 0.70% & 1.00% by volume). All the beams were designed as over-reinforced sections so that the beams fail due to concrete crushing. For the beams reinforced with steel reinforcement, 3 bars of 12 mm diameter are provided on the tension side whereas for the beams with GFRP as internal reinforcement, 12 bars of 12 mm diameter are provided in order to keep the stiffness of both the beams same (equivalent area concept as discussed in Sec. 1.4). On the compression side, 2 GFRP bars each of 12 mm diameter is provided for beams with steel as internal reinforcement. Moreover, for the beams with GFRP bars as internal reinforcement 2 bars each of 12 mm diameter is provided. Reinforcement ratio is kept same on the compression side for all the specimens as the moment contribution from compression bar is minimal. Macro-synthetic polyolefin fibers were used for fiber reinforced concrete. All specimens were 3600 mm long with a rectangular cross-section of 250mm x 300 mm. The details of the test specimen are shown in Table 3. 1. The shear span (a) to depth (d) ratio chosen is 4.9. The beam had a constant moment region of 600mm @ mid-span and shear span (a) of 1350 mm. Steel stirrups of 8 mm diameter were provided only in the shear span at a center to center spacing of 75mm in order to arrest possible shear failure. The test specimen and cross-section details of the beams are illustrated in Figure 3. 1.



(a) Dimensions of the test beam



(b) Beams with steel reinforcement

(c) Beams with GFRP reinforcement

Figure 3. 1: **Beam specimen details** (dimensions in mm)

Table 3. 1: **Test matrix**

Specimen ID	Number of Specimens	Cross-section (mm)	Fiber content (by volume)	Area of bars (tension) (mm ²)	ρ_t (%)	Reinforcement type
ST00	2	250x300	0.00%	3 Φ 12 = 339	0.45	Steel
GF00	2	250x300	0.00%	12 Φ 12 = 1356	1.81	GFRP
GF35	2	250x300	0.35%	12 Φ 12 = 1356	1.81	GFRP
GF70	2	250x300	0.70%	12 Φ 12 = 1356	1.81	GFRP
GF100	2	250x300	1.00%	12 Φ 12 = 1356	1.81	GFRP

3.2 Material Properties

3.2.1 Concrete

The details of mix design are given in Table 3. 3. Concrete was designed as per IS 10262-2008 to have a target cube compressive strength of 40 MPa. The particular value of concrete strength is selected so that capacity of the beam should not go beyond the capacity of the MTS actuator. High Range Water Reducing (HRWR) admixture was used to maintain the workability of concrete mix. Blended coarse aggregates of two different sizes (20 mm: 10 mm = 0.40: 0.60) were used for concreting. In addition, cubes and cylinders were cast to investigate the compression strength and stress-strain behavior of concrete (Figure 3. 2). The results of cube and cylinder tests are summarized in Table 3. 2.

Table 3. 2: Results of cube and cylinder tests under compression

	ST00	GF00	GF35	GF70	GF100
Cube	47.72	48.46	47.69	50.49	51.00
Cylinder	35.79	37.79	41.49	40.39	45.50

*all units are in MPa



Figure 3. 2: Tested cube and cylinder

Table 3. 3: **Details of mix design**

Unit weight (kg/m ³)				
Cement	Fine aggregate	Coarse aggregate	Water	HRWR
360	752	1196	144	5.4

3.2.2 Macro-synthetic polyolefin fibers

The fibers used in FRC are macro-synthetic polyolefin fibers. Polyolefin fibers are non-corrosive and its workability is better when compared to steel fibers. Also, being macro fibers it can arrest the structural cracks. The fibers are of 50 mm in length having a diameter of 0.5mm and were randomly distributed in the concrete mix (Figure 3. 3). Fibers have an aspect ratio of 100. The elastic modulus of the fibers is 10 GPa and tensile strength of 918 MPa. The properties of fibers provided by the supplier are given in Table 3. 4.

Table 3. 4: **Mechanical properties of Polyolefin fibers**

Diameter (mm)	Length (mm)	Aspect ratio	Modulus of Elasticity (GPa)	Tensile strength (MPa)
0.5	50	100	10	918



Figure 3. 3: **Distributing fibers in concrete mix**

3.2.3 Reinforcing Steel bars

Grade of steel which was used for both longitudinal and transverse reinforcement was Fe500. There were total of three longitudinal bars of 12mm diameter provided on the tension side (two on the sides and one at the center) and two on the compression side of the beam to hold the stirrups. Properties of the bar used is given in Table 3. 5.

3.2.4 Reinforcing GFRP bars

GFRP bars used in the beams were 3.5m long. Twelve bars of 12 mm diameter were used on tension side. Bars were placed by tying two bars together and then tying with the stirrups (Figure 3. 4). Two bars were provided on the compression side of the beam to hold the stirrups. Bars have an elastic modulus of 53.5 GPa and a yield strength of 848 MPa. Tensile test was done as per the guidelines provided in ACI 440 (Figure 3. 5). Properties of the bar used is given in Table 3. 5. Figure 3. 6 shows the stress-strain curve obtained for GFRP bars' tension test.



Figure 3. 4: Preparation of reinforcement cages with GFRP bars

Table 3. 5: Mechanical properties of Steel and GFRP bars

Bar type	Diameter (mm)	Area (mm ²)	Modulus of Elasticity (GPa)	Yield strength (MPa)	Tensile strength (MPa)
Steel	12	113.06	200	510	622
GFRP	12	113.06	53.5	----	848



Figure 3. 5: Test setup for tensile test (left) and GFRP bars after failure (right)

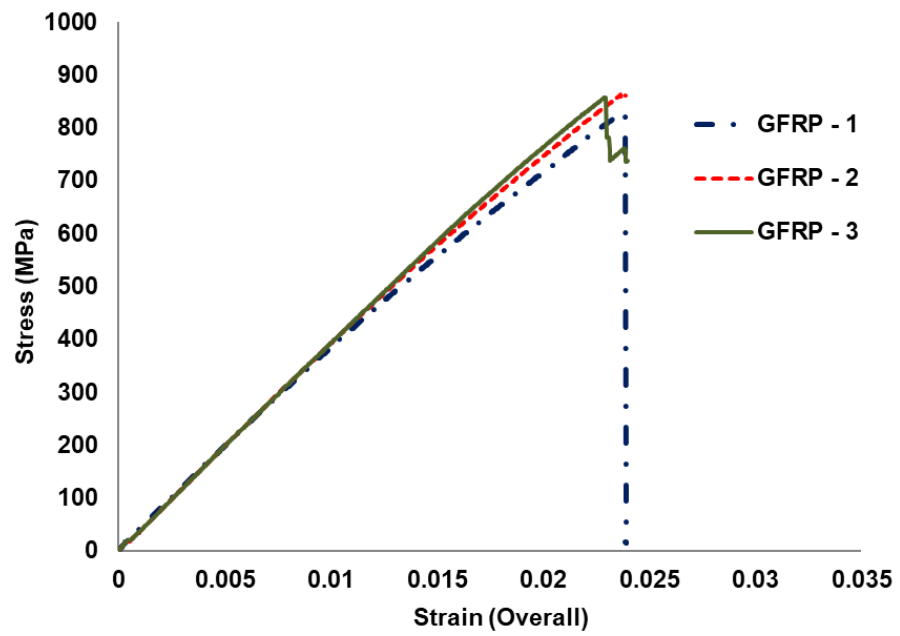


Figure 3. 6: Stress-strain curve for GFRP bars

The specimens are not restrained as they are simply supported and the same is portrayed in the Figure 3. 7. Support width is expected to have minimal influence on the behavior as the specimens are tested at higher a/d ratio of 4.9. All the beams had a test span (constant moment zone) of 600 mm. The beams were simply supported. I – beams was used as loading beams. The load from the MTS actuator was transferred to the loading beams with the help of a spreader beam. The loading beams were placed at a distance of 300 mm one each on both sides from the center of the beam. The effect of different a/d ratio, support conditions, cross section details and size effect on the behavior of fiber reinforced concrete beams would be interesting and is scope for further work. In total 10 beams were cast with different fiber dosages of 0.00%, 0.35%, 0.70% and 1.00% and were water-cured for a period of 28 days at room temperature. The beam schematic and loading configuration are presented in the Figure 3. 7.

3.3.2 Instrumentation

During testing, the specimens are highly instrumented to measure the local and global behavior. Strain gauges are instrumented on the tension and compression reinforcements of the beams during casting. All the beams were tested in a displacement-controlled mode using servo-controlled 250 kN MTS actuator in a closed loop system. The instrumentation details are shown in Figure 3. 8. All the beams were loaded at a rate of 0.05 mm/sec. The loading is paused intermittently at intervals of 10 kN to mark the crack propagations and to observe the failure mechanism while testing. Instrumentations for measuring the data during the loading protocol is carried out with the help of Data Acquisition System (DAQ) connected with Linear Variable Displacement Transducer (LVDT) and strain gauges. Two LVDTs of 100 mm stroke are used at the mid-span to determine the displacement. In addition, two LVDTs of 50mm stroke are used to determine the entire curvature profile of the member. Four LVDT's of 20mm stroke is installed in the horizontal direction to determine the curvature of the section @ mid-span. Digital Image Correlation (DIC) technique is used to monitor the surface strains and crack width at the predefined locations (constant moment zone) where the failure is expected to occur.



1. 250 kN MTS Actuator; 2.HBM DAQ system; 3. DIC camera; 4. DAQ Controller; 5. MTS Controls system; 6. Light source for DIC; 7. Test Specimen

Figure 3. 8: Test setup and Instrumentation Details

Chapter 4

Test results and Discussions

4.1 General

This chapter summarizes the experimental results of the tested specimens. A total of 10 GFRP reinforced concrete beams were tested with varying fiber dosages. The performance of beams with GFRP and steel as internal reinforcement is discussed in this chapter. Also, the role of macro-synthetic polyolefin fibers in increasing the ductility of the beam reinforced with GFRP bars is explained. The results obtained from DIC is highlighted. In addition, various plots such as load vs deflection, moment-curvature, load vs strain and crack width are presented to understand the role of fibers in performance improvement. The effect of fiber ratio on the failure mode is also highlighted in this chapter.

4.2 Load- Deflection Behavior

The load-deflection for all the specimens are discussed in this part of Chapter 4. The results are compared with results obtained from DIC analysis. Also, the overall comparison of the results is reported in this part.

4.2.1 Beams with steel as internal reinforcement without fibers (control specimens)

The steel reinforced specimens were designed to fail in under-reinforced manner. It had a low tension reinforcement ratio of 0.45%. The peak load for the first control specimen (ST00-1) was 89.23 kN while for the second specimen was 89.36 kN. The average peak load for the control specimen observed was 89.3 kN. The first crack appears at a load of around 20 kN and steel bars started yielding at a load of about 70 to 80 kN for both the specimens. The steel rebars yielded before failure. The specimen underwent large ultimate displacement of about 86 mm showing a ductile behavior. Load vs deflection curve is portrayed in Figure 4. 1.

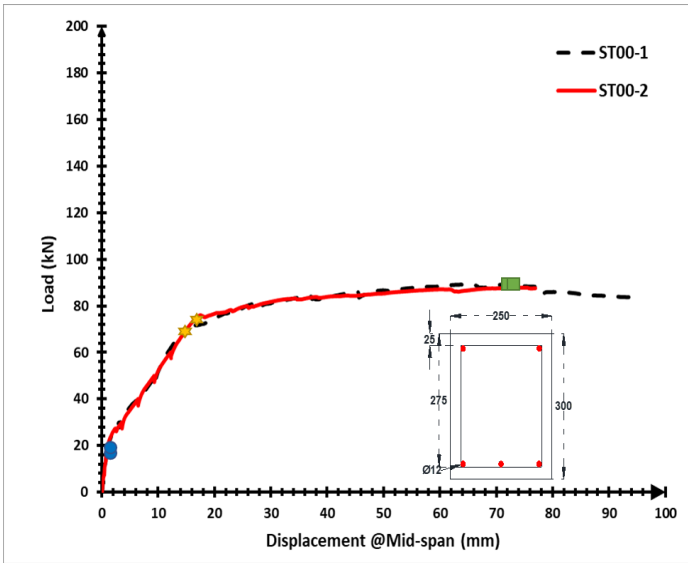


Figure 4. 1: Load vs mid-span deflection for control beams

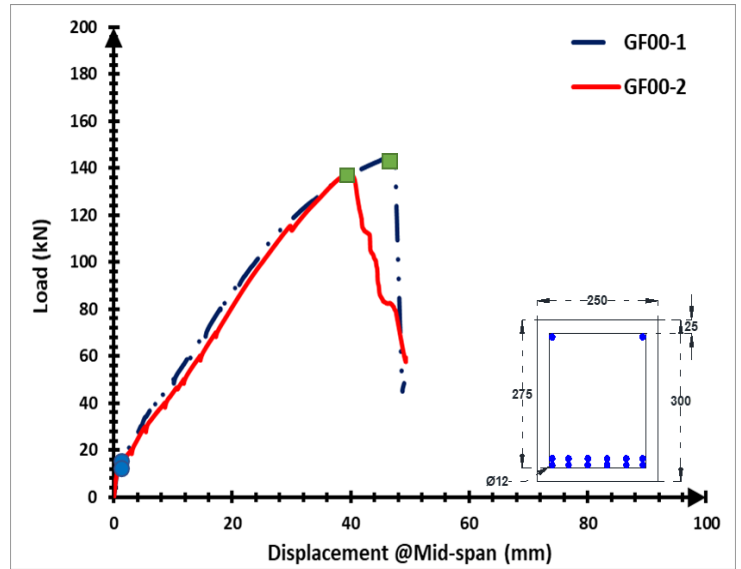


Figure 4. 2: Load vs mid-span deflection for beams with GFRP without fibers

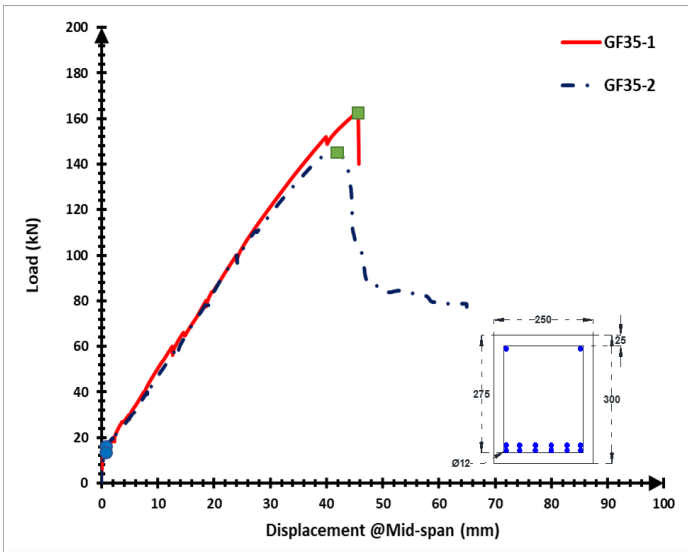


Figure 4. 3: Load vs mid-span deflection for beams with GFRP with 0.35% fibers

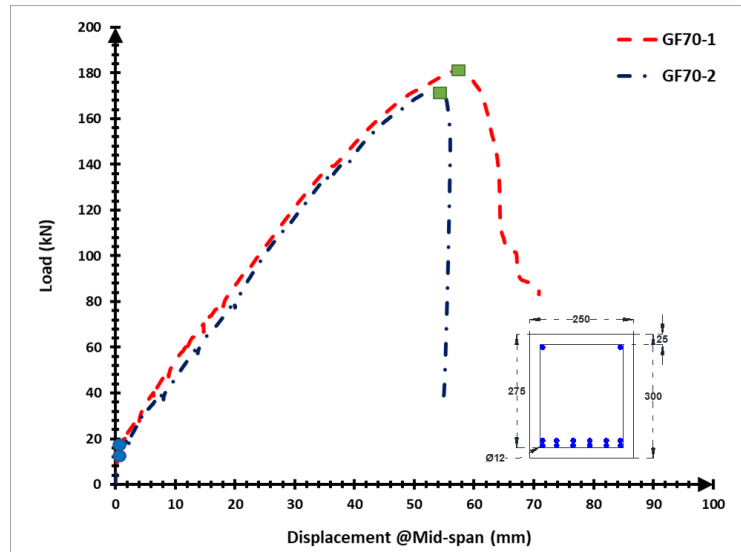


Figure 4. 4: Load vs mid-span deflection for beams with GFRP with 0.70% fibers

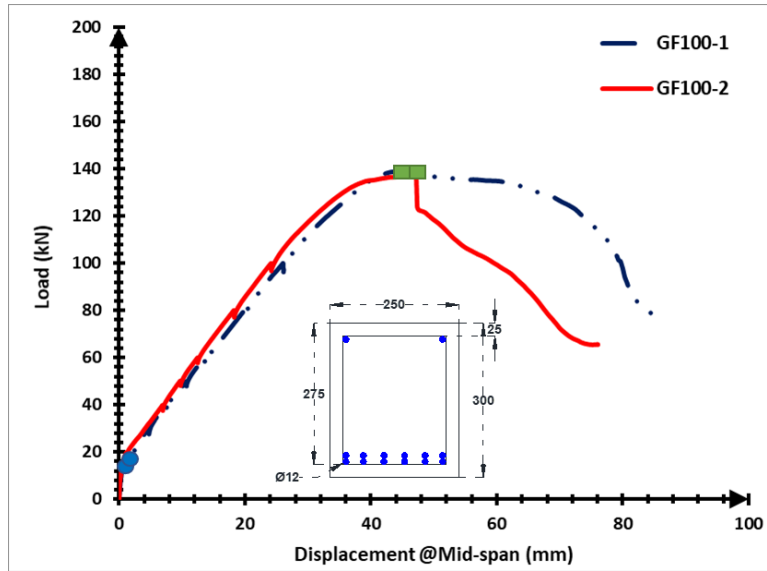


Figure 4. 5: Load vs mid-span deflection for beams with GFRP with 1% fibers

- - Cracking load
- ★ - Yielding load
- - Peak load

4.2.2 Beams with GFRP as internal reinforcement without fibers

All the GFRP reinforced specimens had a tension reinforcement ratio of 1.82%. Typically, RC specimens will have a balanced failure within reinforcement ratio of 2.5 to 3.0% depending on the concrete strength. However, this limit may not be applicable for GFRP reinforced beams. When the steel reinforcement is replaced with GFRP equivalent area, the beam had peak load capacity of 141.3 kN which is around 59.2% improvement when compared to the steel reinforced specimen. However, the beam had a severe reduction in ultimate displacement. It failed at 49 mm displacement which is only 24% with respect to steel specimens. The beam failed suddenly as soon as it reached its peak load and did not show any ductility. Load vs deflection curve for this set of beams is illustrated in Figure 4. 2.

4.2.3 Beams with GFRP as internal reinforcement with 0.35% fibers

For beams reinforced with GFRP bars and 0.35% PO fibers, the peak load capacity is found to be 154.1 kN. When compared to steel reinforced beams, the load capacity increased by 72.6%. The

ultimate displacement was found to be 56 mm which is only 46% of the steel reinforced beams. Beams showed some ductility when compared to beams reinforced with GFRP bars without fibers. Load vs deflection curve for this set of beams is presented in Figure 4. 3.

4.2.4 Beams with GFRP as internal reinforcement with 0.70% fibers

For beams with 0.70% fiber addition, the peak load improvement is more than 100% when compared to beam with steel reinforcement. Moreover, the ultimate displacement is restored by 79% when compared to steel reinforced beams. Load vs deflection curve for this set of beams is plotted in Figure 4. 4.

4.2.5 Beams with GFRP as internal reinforcement with 1% fibers

When the beams are added with 1% fiber dosage, the peak strength is about 138 kN which is 55% higher than steel reinforced beams. It is worth mentioning that, beams had negligible strength improvement when compared to GF00 specimens. However, the ultimate displacement ductility is restored completely. Load vs deflection curve for this set of beams is presented in Figure 4. 5.

4.2.6 Overall Comparison

The overall comparison of beams is shown in Figure 4. 6. Replacement of steel with equivalent GFRP as longitudinal reinforcement resulted in significant strength improvement but a cost of sudden brittle failure and reduced ultimate displacement. However, the addition of fibers significantly improved the ultimate displacement and energy absorption capacity of the beams. With the addition of 0.70% fibers, beams showed good load carrying capacity. At 1% PO fiber addition, the ductility is completely restored similar to steel reinforced RC beams. The failure mode is changed from brittle over-reinforced failure (GF00) to ductile flexure mode (GF100). With the results, we can also say that with high fiber dosage reduces the strength of the beams. This could be due to the bundling of fibers resulting in less cohesion of fibers with concrete at the tension region which resulted in quicker crack propagation and changed the failure progression. Summary of the results is presented in Table 4. 1.

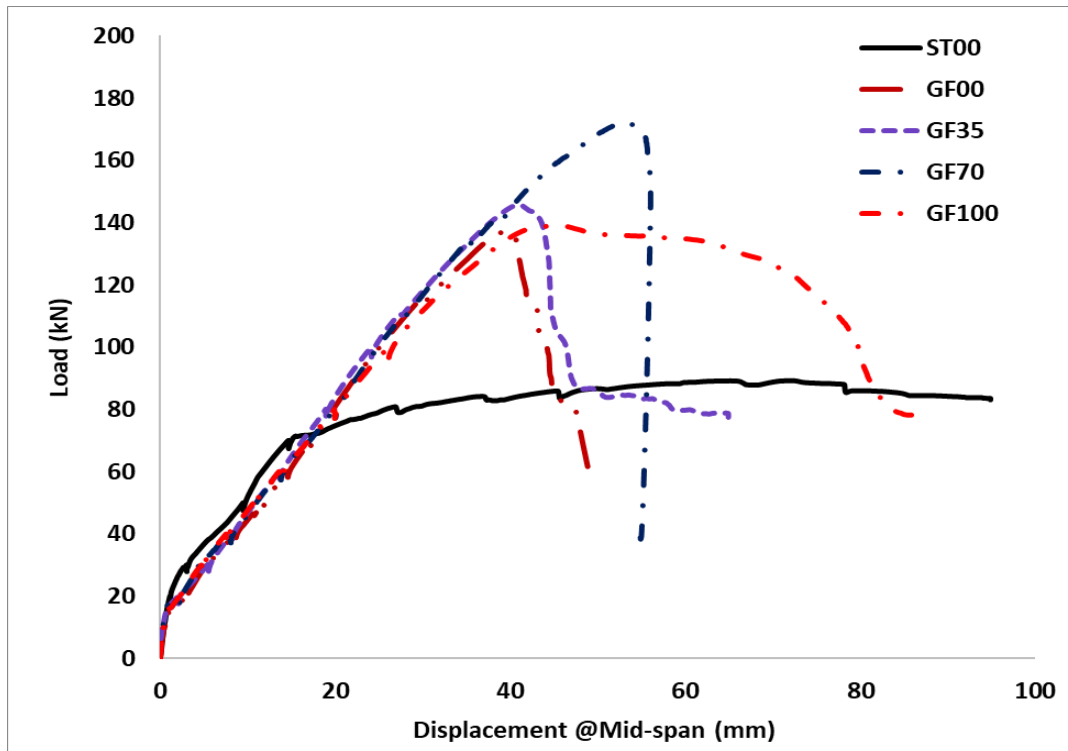


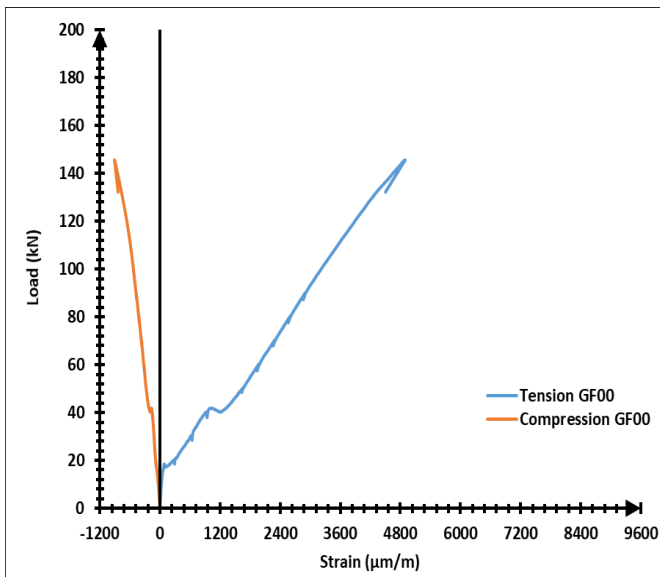
Figure 4. 6: Overall load vs displacement comparison

Table 4. 1: Summary of test results

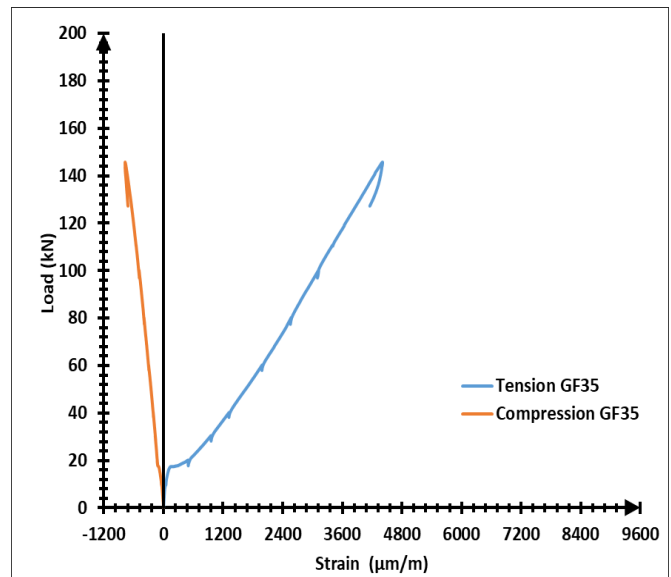
Parameters	ST00-1	ST00-2	GF00-1	GF00-2	GF35-1	GF35-2	GF70-1	GF70-2	GF100-1	GF100-2
Cracking Load (kN)	19.02	18.74	18.48	16.23	16	17.11	19.18	16.90	15.12	18.47
Deflection at cracking load (mm)	1.01	1.02	1.06	1.04	0.53	0.88	1.18	0.73	0.73	1.22
Peak Load (kN)	89.23	89.39	145.65	137.48	162.61	145.67	180.80	171.99	139.01	137.13
Increase in peak load (%)	--	--	62.50	53.41	82.09	63.12	102.5	92.6	55.65	53.41
Deflection at peak load (mm)	71.89	76.88	47.42	39.71	45.51	40.92	56.56	52.97	45.72	45.69
Deflection at failure load (mm)	94.85	76.88	49.01	49.23	45.75	64.90	70.86	55.15	86.31	75.99
Strain energy (Joule)	7394	5883	4509	4060	4281	5665	8149	5820	8874	6997
Increase in strain energy (%)	--	--	-32	-38.8	-35.5	-14.7	22.7	-12.3	33.7	5.4

4.3 Load – Strain

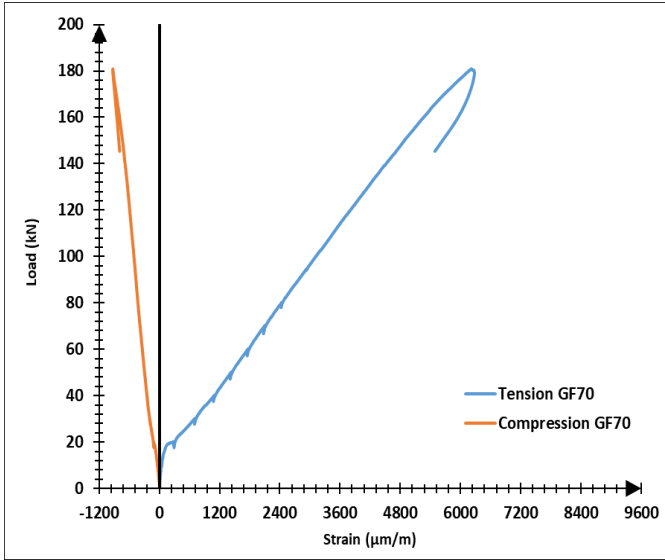
Load vs strain for all the beams have been plotted in Figure 4. 7. Both the compression and tension strains have been plotted. Strain gauges were placed in the center of the bar. From the plots we can see that for the beams with GFRP without fibers (Figure 4. 7 (a)) and with 0.35% fibers (Figure 4. 7 (b)) are failing as soon as it reaches its peak load whereas beam with 0.70% and 1% fibers (Figure 4. 7 (c) & (d)) is showing some ductility. Beam with steel bars (Figure 4. 7 (e)) are showing very good ductility. Overall comparison of load vs strain is shown in Figure 4. 7 (f).



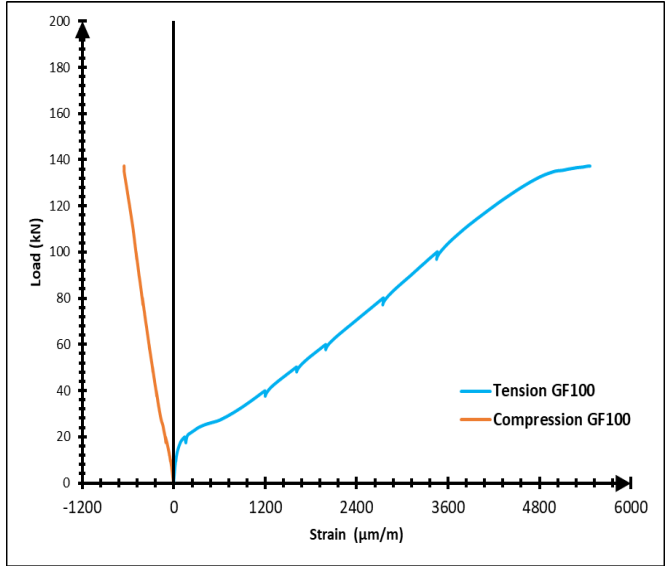
(a) Beams with GFRP without fibers



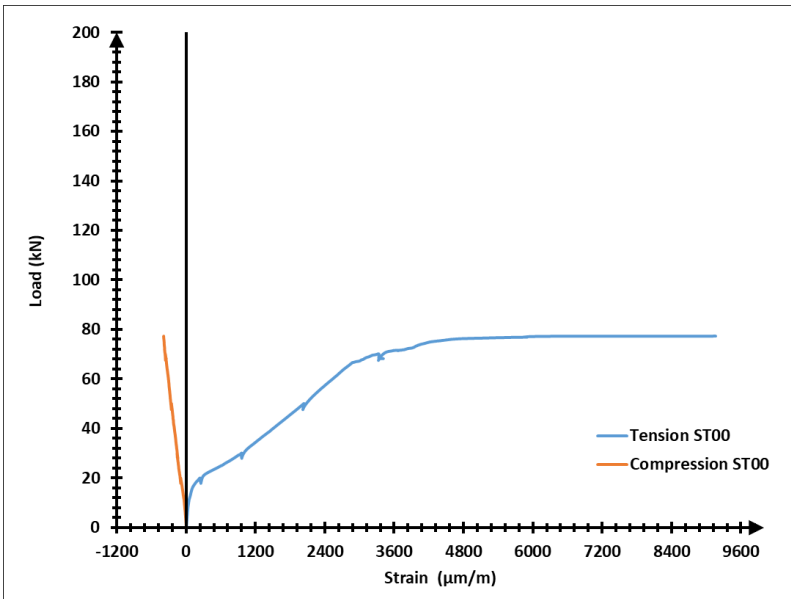
(b) Beams with GFRP with 0.35% fibers



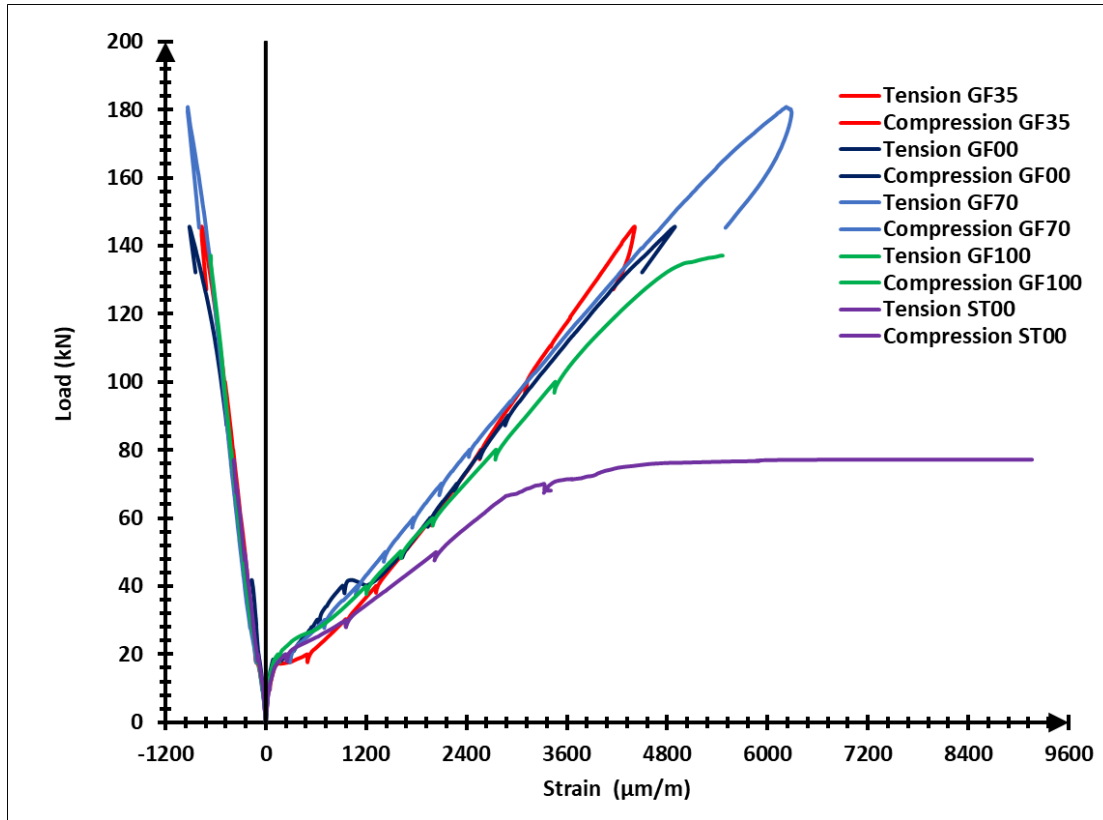
(c) Beams with GFRP with 0.70% fibers



(d) Beams with GFRP with 1% fibers



(e) Beam with steel



(f) Overall comparison for beams with GFRP

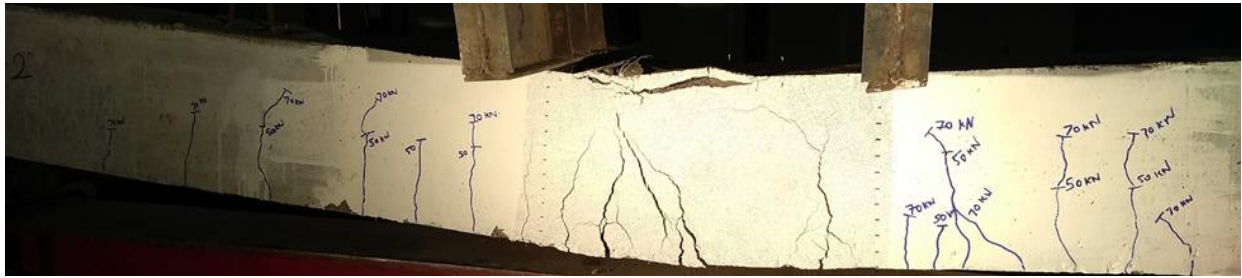
Figure 4. 7: **Load versus strain**

4.4 Failure mode comparison

Beams with steel bars failed by crushing of concrete at the compression side (Figure 4. 8 (a)) under flexure as the beams designed were heavily under reinforced. For the beams with GFRP bars without fibers, failure zone shifted from constant moment zone to shear span and failed in flexure shear mode (Figure 4. 8 (b)). Beams with fiber content of 0.35%, the failure is due to the flexure shear mode with the sudden crack development in the shear span zone (Figure 4. 8 (c)). Beams with a fiber content of 0.70% failed in flexure shear mode (Figure 4. 8 (d)). The failure zone shifted from constant moment zone to shear span. However, the beams with 1.0% fiber content failure mode changed from brittle over-reinforced type to ductile flexure mode (Figure 4. 8 (e)). Table 4. 2 summarizes the types of failure observed for the different set of beams.

Table 4. 2: Summary of Failure modes

Series name	Failure Mode
ST00	Flexure Mode
GF00	Flexure – Shear Mode
GF35	Flexure – Shear Mode
GF70	Flexure – Shear Mode
GF100	Flexure Mode



(a) Steel Reinforced Beam



(b) GFRP Reinforced Beam



(c) GFRP Reinforced Beam with 0.35% PO Fiber



(d) GFRP Reinforced Beam with 0.70% PO Fiber

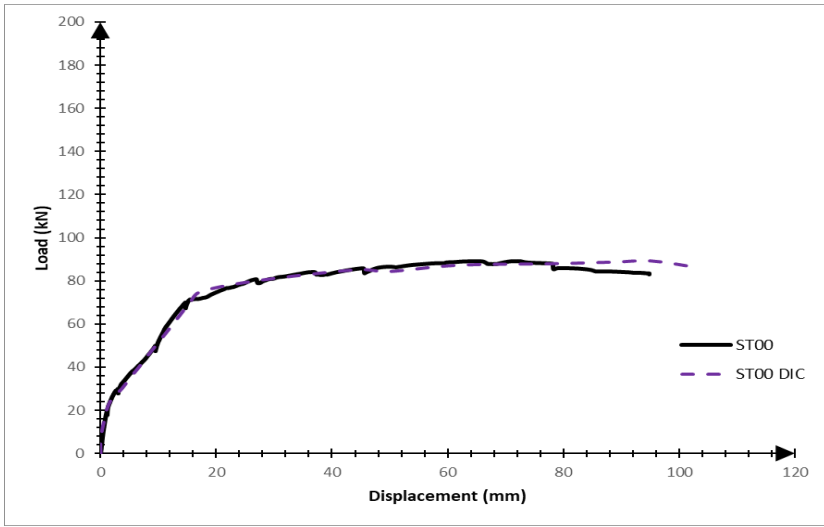


(e) GFRP Reinforced Beam with 1.0% PO Fiber

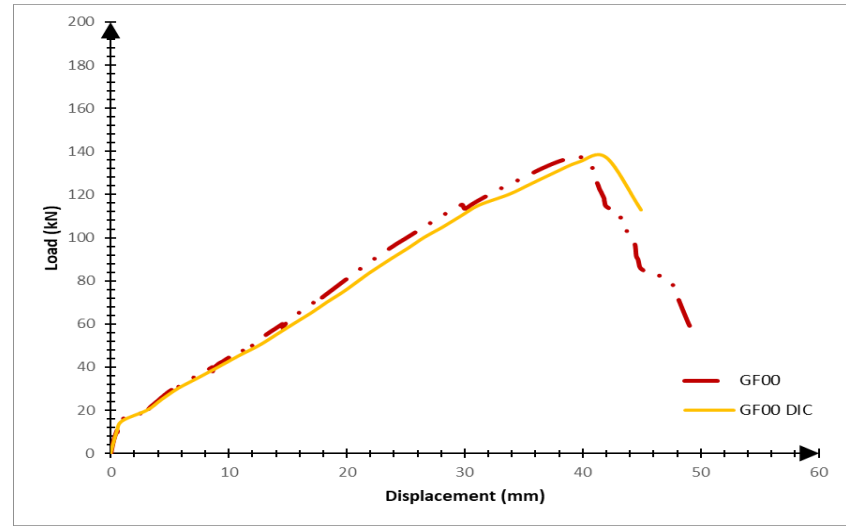
Figure 4. 8: Failure Mode Comparisons for RC Beams

4.5 Load-Displacement comparison (DIC & LVDT)

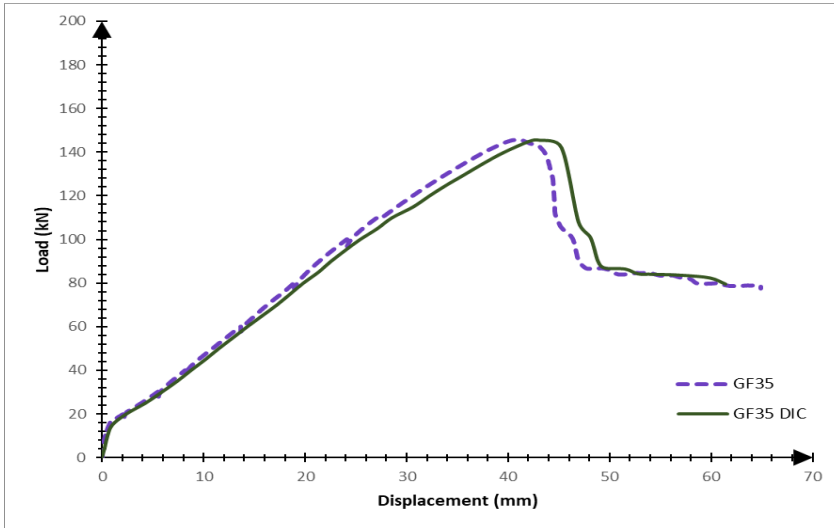
Mid-span deflection is obtained by the analysis of images captured through DIC camera and compared to the data obtained from LVDTs placed at the mid-span of the beam. Load-deflection data from DIC shows very good agreement with the data obtained from LVDTs through DAQ. Figure 4. 9 shows comparison of data obtained from LVDT and DIC.



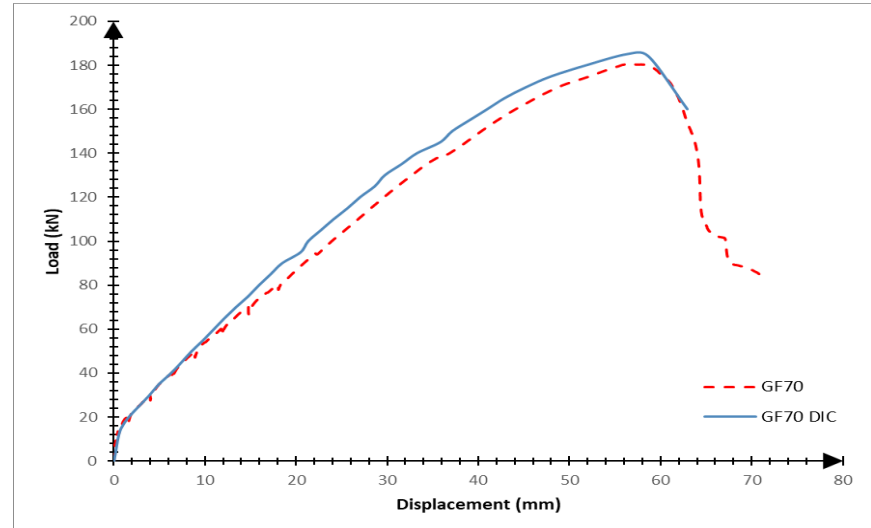
(a) Beam with steel bars



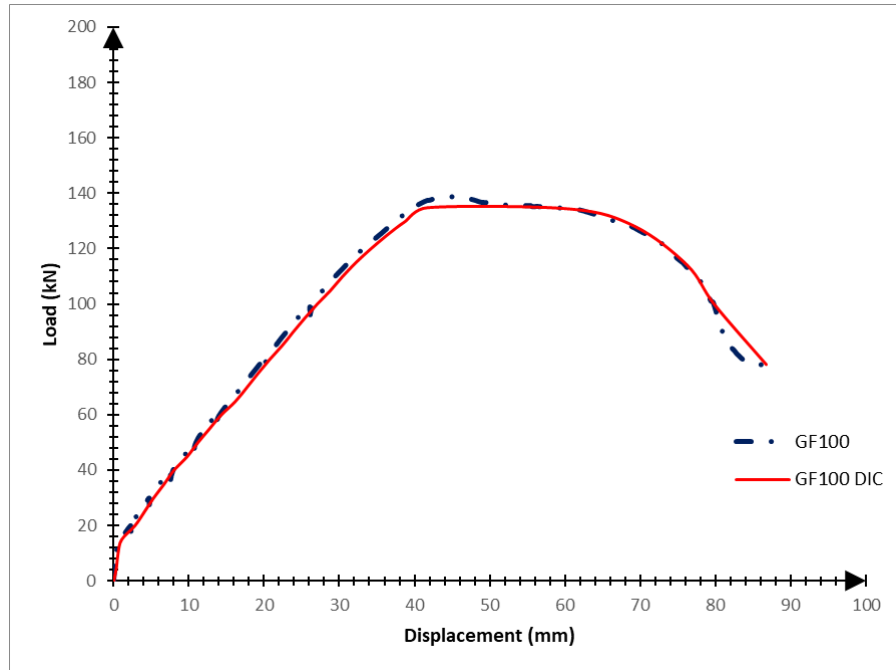
(b) Beam with GFRP bars without fibers



(c) Beam with GFRP bars with 0.35% PO fibers



(d) Beam with GFRP bars with 0.70% PO fibers



(e) Beam with GFRP bars with 1% PO fibers

Figure 4. 9: Load-displacement comparison (DIC & LVDT)

4.5 Crack width comparison

Figure 4. 10 shows crack width comparison for beams reinforced with GFRP bars. Crack width was one of the most important aspects which needs to be considered when using brittle reinforcing materials like GFRP bars as they show higher crack width when compared to traditional steel reinforcing bars. The crack width was captured in the constant moment zone and the values are plotted for the crack with higher crack width when there is more than one crack. Also, if the cracks are of nearly equal widths, average crack width was taken. Crack width was obtained at the level of tension reinforcement, i.e., a distance of 25mm from the bottom, using DIC. The crack width is obtained at 25%, 50%, 75% and at the peak load of the beam. We conclude from the analysis that with the increase of fiber dosage, the crack width reduces. So, use of FRC is a good way to reduce the crack width of the beams with GFRP bars as internal reinforcement. Figure 4. 11 shows contour plot of the beams at a load of 80kN.

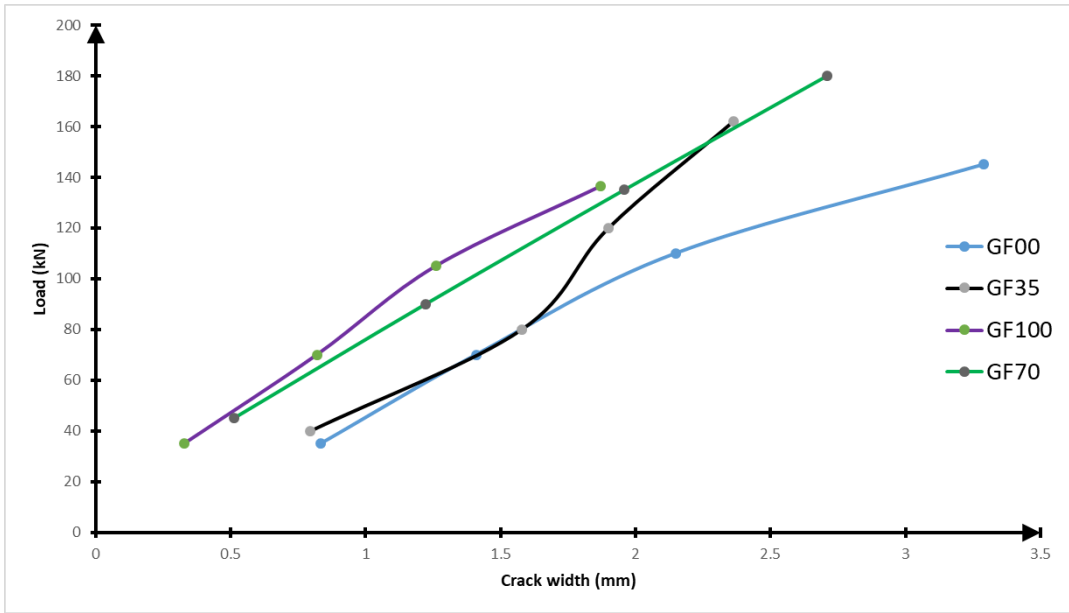


Figure 4. 10: Load vs Crack width

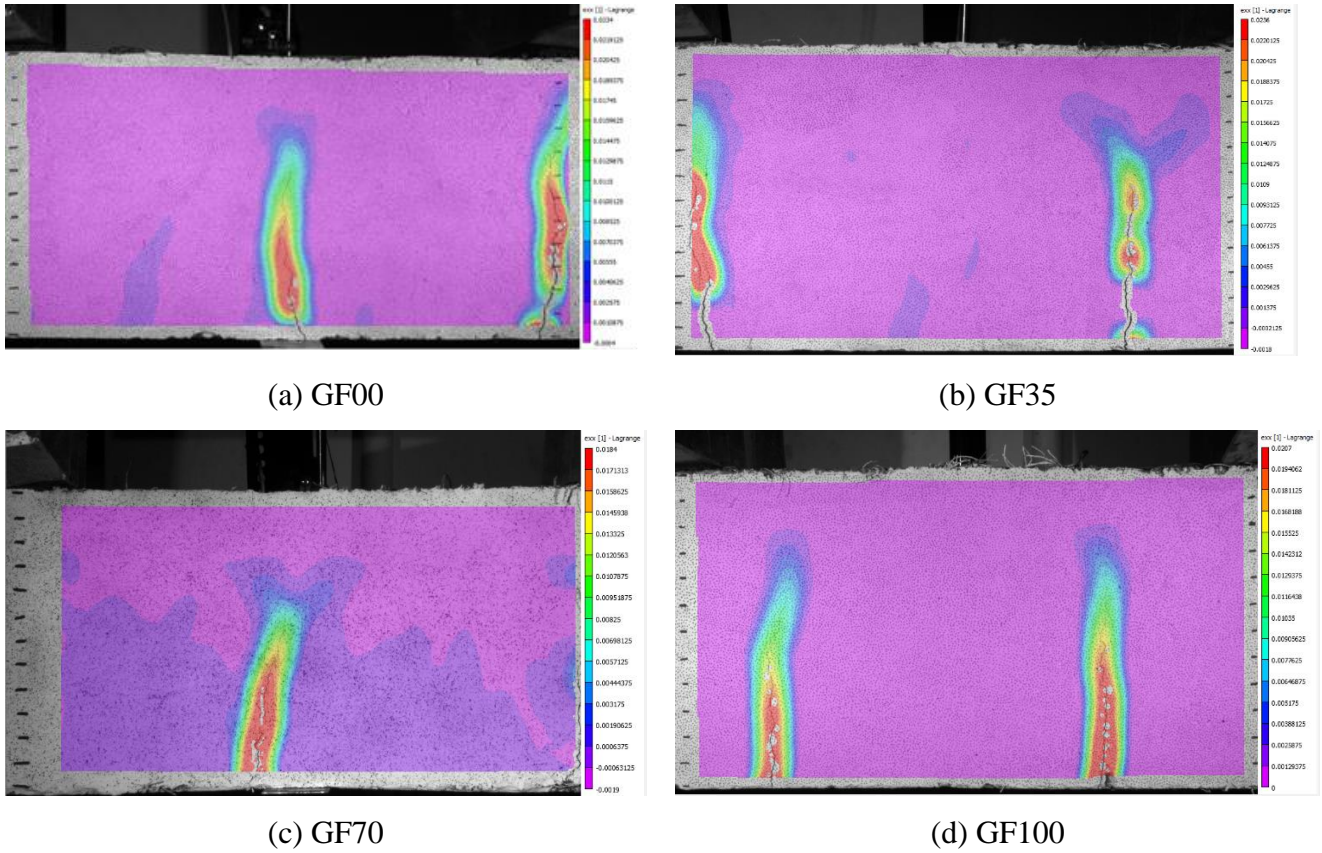


Figure 4. 11: Contour of beams

Chapter 5

Analytical Study

5.1 Analytical model for Moment-curvature predictions

5.1.1 General

For the analytical study for moment-curvature, the stress-strain curve model proposed by Chang et al. (2012) for fiber reinforced concrete is considered. They used the parabolic model for plain concrete in compression proposed by Carreira and Chu (1985) with some modifications incorporating the effect of fibers in concrete. In the current study, the model proposed by Chang et al. (2012) is modified to predict the compressive behavior of concrete reinforced with macro synthetic polyolefin fibers.

5.1.2 Carreira and Chu model for plain concrete in compression

$$\frac{f_c}{f'_c} = \frac{\beta \left(\frac{\varepsilon}{\varepsilon'_c}\right)}{\beta - 1 + \left(\frac{\varepsilon}{\varepsilon'_c}\right)^\beta} \quad (1)$$

where

$$\beta = \frac{1}{1 - \frac{f'_c}{E_{it}\varepsilon'_c}} \quad (2)$$

Here, β is a material parameter depends on the shape of the stress-strain diagram. The variables used in the equations are defined in the nomenclature. Chang et al. (2012) used this model to develop his model for concrete with steel fibers in compression.

5.1.3 Chang et al. (2012) model for concrete with steel fibers in compression

Chang et al. (2012) in his model used the same parabolic model which Carreira and Chu proposed for plain concrete. But they modified the equation for β . In their modified equation of β , they showed β to be a function of reinforcing index. Reinforcing index, on the other hand, depends on the volume fraction of fiber used, length of the fiber and diameter of the fiber. They also modified the compressive strength of the concrete and strain at the peak stress and made it a function of reinforcing index. The modified model proposed is given below:

$$\frac{\sigma_c}{f'_{cf}} = \frac{\beta \left(\frac{\epsilon_c}{\epsilon_{cf}} \right)}{\beta - 1 + \left(\frac{\epsilon_c}{\epsilon_{cf}} \right)^\beta} \quad (3)$$

where,

$$f'_{cf} = f'_c + 2.35(RI_v) \quad (4)$$

$$\epsilon_{cf} = \epsilon_{c0} + 0.0007(RI_v) \quad (5)$$

$$\beta = 0.71(RI_v)^2 - 2.00(RI_v) + 3.05 \quad (5)$$

$$RI_v = V_f^* \frac{l}{\phi} \quad (6)$$

5.1.4 Proposed model for concrete with macro-synthetic polyolefin fibers

The model used in this study used the same equations proposed by Chang et al. (2012) in their model for f'_{cf} , ϵ_{cf} and β . Chang et al. (2012) model was improved using a modification factor of 0.5 to simulate the behavior with respect to the experiments. The proposed model is given below:

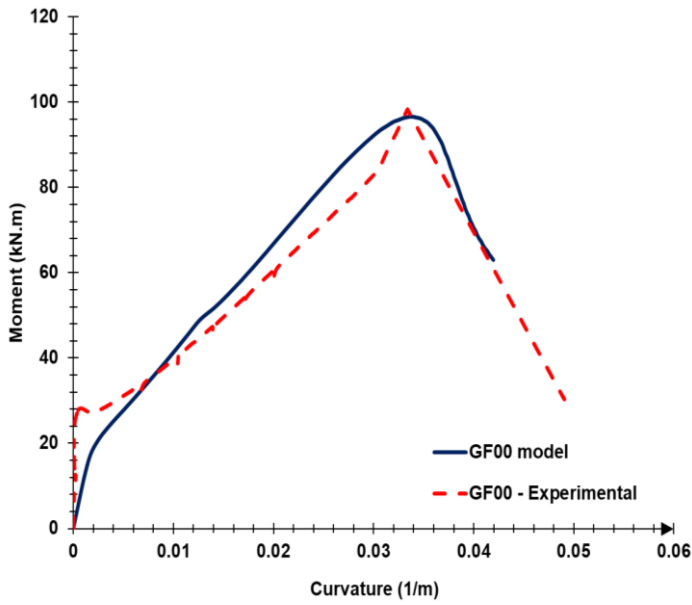
$$\frac{\sigma_c}{f'_{cf}} = \frac{0.5\beta \left(\frac{\epsilon_c}{\epsilon_{cf}} \right)}{\beta - 1 + \left(\frac{\epsilon_c}{\epsilon_{cf}} \right)^\beta} \quad (7)$$

5.1.5 Comparison of the test result and analytical predictions

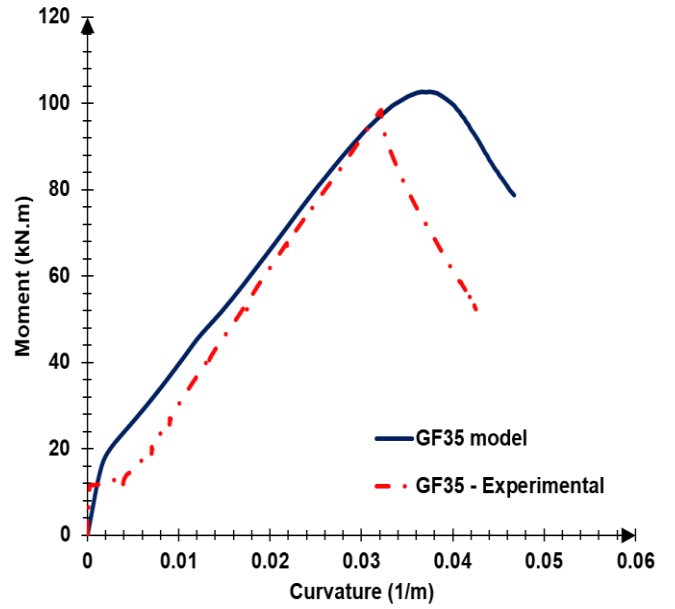
The model proposed shows good agreement with the experimental results except for the beams with 1% fiber dosage. As mentioned earlier, with high fiber dosage strength of the beam reduces and hence, the experimental result doesn't show good agreement with 1% fiber dosage. Figure 5. 1 shows comparison of moment curvature plot for experimental results and proposed analytical model. Table 5. 1 summarizes the result obtained from analytical model and experimental results.

Table 5. 1: Comparison of analytical and experimental results

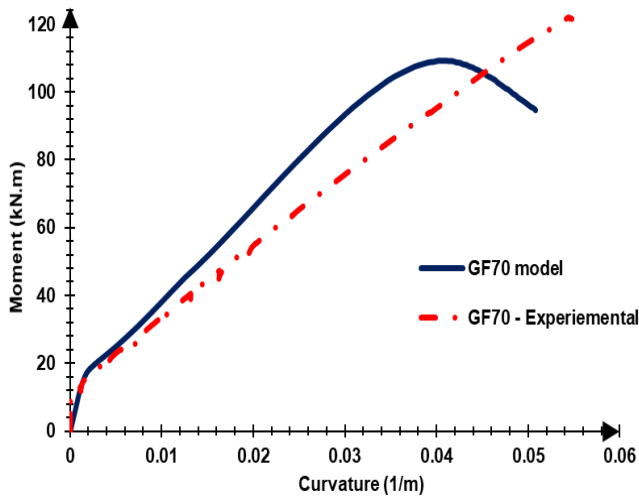
Specimen ID	Experimental		Analytical		M_{exp}/M_{an}
	Peak Moment (M_{exp}) (kNm)	Curvature at peak moment (1/m)	Peak Moment (M_{an}) (kNm)	Curvature at peak moment (1/m)	
GF00	98.3117	0.03340	96.52	0.03395	1.02
GF35	98.33	0.03217	102.68	0.03748	0.96
GF70	120.416	0.05349	109.05	0.04058	1.09
GF100	92.738	0.02959	114.79	0.04435	0.81



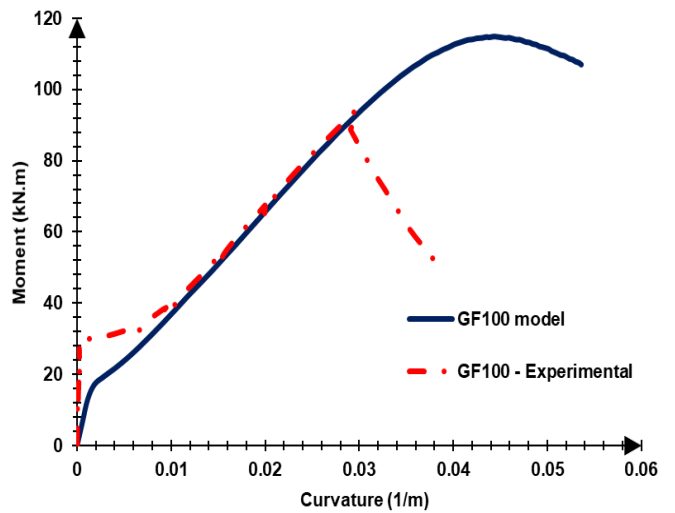
(a) Beam with GFRP bars without fibers



(b) Beam with GFRP bars 0.35% PO fibers



(c) Beam with GFRP bars with 0.70% PO fibers



(d) Beam with GFRP bars with 1% PO fibers

Figure 5. 1: Moment-curvature comparison

5.2 Analytical model for load – deflection predictions

5.2.1 General

For conventional FRP bar reinforced concrete beams, the concrete contribution in the tension zone is usually neglected after cracking. However, in the case of FRC beams reinforced with FRP bars, as the tensile stress can be carried by the fibers in cracked section, the contribution of fibers in the cracked section must be considered. For load-deflection predictions, we used the model proposed by Haitang Zhu et al. (2017) for fiber reinforced concrete with FRP bars to calculate deflection in the beam under flexure. Zhu in his model modified the model proposed by ACI 440.1R-15 which was applicable for plain concrete.

5.2.2. ACI 440.1R-15 model

ACI 440.1R-15 suggests that the deflection caused in a beam under flexure can be calculated by the equation given below:

$$\Delta = \frac{PS}{48E_cI_e} (3L^2 - 4S^2) \quad (8)$$

Variables used are defined in nomenclature. ACI 440.1R-15 suggests I_e i.e., effective moment of inertia, can be calculated by Eq. (9).

$$I_e = \frac{I_{cr}}{1 - \gamma \left(\frac{M_{cr}}{M_a}\right)^2 \left(1 - \frac{I_{cr}}{I_g}\right)} \leq I_g \quad \text{where } M_a \geq M_{cr} \quad (9)$$

where,

$$\gamma = 1.72 - 0.72 \left(\frac{M_{cr}}{M_a}\right) \quad (10)$$

$$I_g = \frac{bh^3}{12} \quad (11)$$

$$I_{cr} = \frac{b}{3} d^3 k^3 + n_f A_f d^2 (1 - k)^2 \quad (12)$$

$$k = \sqrt{2\rho n_f + (\rho n_f)^2} - \rho n_f \quad (13)$$

ACI 440.1R-15 assumes that before cracking of concrete, the section is homogenous and the contribution of reinforcement to the moment of inertia of the gross section is negligible and is given by Eq. (11). Also, based on the assumption that the concrete contribution in the tension zone can be neglected after the cracking of concrete ACI 440.1R-15 suggests that the moment of inertia of cracked section can be calculated by Eqs. (12) and (13).

5.2.3 Haitang Zhu et al. (2017) model

Zhu et al. (2017) in his model, included the contribution of fibers in the calculation of moment of inertia of the cracked section and gross section. Since the distance of the centroid of every single fiber from the neutral axis of the beam is unknown the area and moment of inertia of a single fiber cannot be calculated. To obtain the area and moment of inertia of fibers, the fibers can be considered as a whole. The average distance of the steel fibers in compression zone from the neutral axis is considered 0.5 times of the depth of compression zone and the average distance of steel fibers in tension zone from the neutral axis is considered 0.5 times of the depth of tension zone. Based on these considerations, gross and cracked moment of inertia can be calculated by Eq. (14) and (17) respectively.

$$I_g = \frac{b}{3} [x_0^3 + (h - x_0)^3] + (n_f - 1)A_f(d - x_0)^2 + \frac{n_{sf}-1}{3h} A_{sf} [x_0^3 + (h - x_0)^3] \quad (14)$$

where,

$$x_0 = \frac{\frac{1}{2}bh^2 + (n_f - 1)A_f d + \frac{n_{sf} - 1}{2} A_{sf} h}{bh + (n_f - 1)A_f + (n_{sf} - 1)A_{sf}} \quad (15)$$

The total area of steel fiber can be calculated by the Eq. (16), where the factor 0.16 is the effective coefficient of the fibers which includes non-uniformity of fiber distribution and orientation of fibers (Gao, 1992).

$$A_{sf} = 0.16bh\rho_{sf} \quad (16)$$

$$I_{cr} = \frac{b}{3}x_{cr}^3 + n_f A_f (d - x_{cr})^2 + \frac{n_{sf} - 1}{3h} A_{sf} x_{cr}^3 + \frac{n_{sf}}{3h} A_{sf} (h - x_{cr})^3 \quad (17)$$

where,

$$x_{cr} = \frac{-(n_f A_f + n_{sf} A_{sf}) + \sqrt{(n_f A_f + n_{sf} A_{sf})^2 + 2(b - \frac{A_{sf}}{h})(n_f A_f d + \frac{n_{sf}}{2} A_{sf} h)}}{b - \frac{A_{sf}}{h}} \quad (18)$$

5.2.4 Comparison of test results with analytical predictions

Based on Zhu's model deflection was calculated at service loads and compared with deflection values from experiment results for the given load values. The experimental and theoretical deflections at service load are shown in Table 5. 2. The model developed by Zhu shows good agreement with the experimental results.

Table 5. 2: Comparison of experimental and theoretical deflections at service load

Specimen	F _{sc} (kN)	Δ _e (mm)	Δ _t (mm)	$\frac{\Delta_e}{\Delta_t}$
		Experimental	Theoretical	
GF00-1	87.35	19.93	19.38	1.03
GF00-2	82.49	20.33	18.11	1.12
GF35-1	97.54	23.32	21.98	1.06
GF35-2	87.40	20.74	19.36	1.07
GF70-1	108.45	26.35	24.73	1.06
GF70-2	103.17	25.68	23.39	1.10
GF100-1	83.41	21.03	18.27	1.15
GF100-2	82.20	19.07	17.95	1.06

Chapter 6

Summary and Conclusions

Ten RC beams were cast and tested as part of this study to understand the effect of structural macro-synthetic fibers on the flexural behavior. Beams were tested in a four-point bending configuration. Shear span to effective depth (a/d) ratio of 4.9 is selected in this study to have predominant bending dominant behavior. DIC technique was used to measure the crack width and deflection of the beams along with conventional displacement sensors (LVDTs). The following major conclusions can be drawn from the results presented and discussed in this work:

Steel vs GFRP as Internal Reinforcement:

- When steel reinforcements are replaced with GFRP bars of equivalent area ($E_s A_s = E_f A_f$), the failure mode changed from flexure to flexure-shear. However, the load carrying capacity of the beam increased significantly when GFRP bars replaced steel of equivalent area.
- Due to low-tension reinforcement ratio, the steel reinforced beams failed in flexure due to crushing of concrete at the compression side after the yielding of tension reinforcement. Moreover, the specimen underwent larger deflection before failure.
- Equivalent area of replacing steel with GFRP bars resulted in change of failure mode from flexure mode to flexure - shear.

Effect of Addition of Fibers:

- Addition of fibers improved the ductility of the beams and reduced the brittle failure nature of the GFRP reinforced beams.
- GFRP reinforced beams exhibited good improvement in strength and strain energy absorption till a fiber volume fraction of 0.7%.

Effect of High Fiber Dosage:

- Addition of 1% of poly-olefin fiber changed the failure mode again from brittle over-reinforced mode to ductile flexure mode. Moreover, the ductility beams are completely restored with good strength improvement when compared to steel reinforced beams.
- It is worth mentioning that 1% addition converted the failure mode from flexure – shear to flexure.
- The ultimate strength of the beam reduced at higher fiber dosage. This could be due to the bundling of fibers resulting in less cohesion of fibers with concrete at the tension region, which resulted in quicker crack propagation and changed the failure progression.

Crack Width Measurements using DIC:

- The load-displacement data obtained from DIC showed good agreement with the test data obtained from DAQ.
- The data obtained from crack width analysis signifies that, with the increase of fiber dosage crack width reduces for any load.

Analytical Studies:

- The proposed analytical model for moment curvature predictions shows good agreement with the experimental results except for the beams with 1% polyolefin fibers as the experimental result shows reduction in load carrying capacity with high fiber dosage. Also, with the increase of fiber dosage, the curvature at the peak moment was also observed to be increasing.
- Deflection predictions at service load levels matched closely with test results. This indicates that the analytical approach presented in this study can be used to predict the deflections of the GFRP reinforced beams at different fiber dosages.

References

1. Nanni, A., “Flexural Behavior and Design of RC Members Using FRP Reinforcement,” *Journal of Structural Engineering*, (1992) V. 119, No. 11, 1993, pp. 3344 – 3359.
2. Toutanji, H. A., and Saafi, M., “Flexural Behavior of Concrete Beams Reinforced with Glass Fiber – Reinforced Polymer (GFRP) Bars,” *ACI Structural Journal*, V. 97, No. 5, Nov. – Dec. 1998, pp. 712 – 719.
3. R. Masmoudi, M. Thériault, B. Benmokrane, “Flexural behavior of concrete beams reinforced with deformed fiber reinforced plastic reinforcing rods”, *ACI Struct. J.* 95 (6) (1998) 665–676.
4. F. Elgabbas, E.A. Ahmed, B. Benmokrane, “Experimental testing of basalt-fiber reinforced polymer bars in concrete beams”, *Compos. Part B Eng.* 91 (2016) 205–218.
5. Mohamed, H., Afifi, M., and Benmokrane, B. (2014). “Performance evaluation of concrete columns reinforced longitudinally with FRP bars and confined with FRP hoops and spirals under axial load.” *J. Bridge Eng.*, 10.1061/(ASCE)BE.1943-5592.0000590, 04014020.
6. D. Deitz, I. Harik, H. Gesund, “Physical properties of glass fiber reinforced polymer rebars in compression”, *J. Compos. Constr.* 7 (4) (2003) 363–366.
7. L. Zhang, Y. Sun, W. Xiong, “Experimental study on the flexural deflections of concrete beam reinforced with Basalt FRP bars”, *Mater. Struct.* 48 (10) (2015) 3279–3293.
8. H. G. Harris, W. Somboonsong, F.K. Ko, “New ductile hybrid FRP reinforcing bar for concrete structures”, *ASCE J. Compos. Constr.* 2 (1) (1998) 28–37
9. S.H. Alsayed, A.M. Alhozaimy, “Ductility of concrete beams reinforced with FRP bars and steel fiber”, *J. Compos. Mater.* 33 (19) (1999) 1792–1806.
10. W.K. Lee, D.C. Jansen, K.B. Berlin, L.E. Cohen, “Flexural cracks in fiber-reinforced concrete beams with fiber-reinforced polymer reinforcing bars”, *ACI Struct. J.* (2010) 321–329.
11. Indian Standards 10262: Recommended Guidelines for Concrete Mix Design. Bureau of Indian Standards 2009, New Delhi.
12. Gao Danying, “Basic Theory of Steel Fiber Reinforced Concrete [M], Scientific and Technical Documentation Press, Beijing, 1994
13. ACI (American Concrete Institute). (2015). “Guide for the design and construction of concrete reinforced with FRP bars.” ACI 440.1R-15, Farmington Hills, MI.

14. CSA (Canadian Standards Association). (2012). "Design and construction of building components with fiber reinforced polymers." CAN/CSA S806-12, Rexdale, ON, Canada.
15. De Luca, A., Matta, F., and Nanni, A. (2010). "Behavior of full-scale glass fiber-reinforced polymer reinforced concrete columns under axial load." *ACI Struct. J.*, 107(5), 589–596.
16. H. Wang; A. Belarbi, "Ductility characteristics of fiber – reinforced – concrete beams reinforced with FRP rebars", *Construction and Building Materials* 25 (2010) 2391-2401
17. H. Zhu; S. Cheng; D. Gao; Sheikh M. Neaz; C. Li, "Flexural behaviour of partially fiber – reinforced high – strength concrete beams reinforced with FRP bars, *Construction and Building Materials* 161 (2018) 587-597
18. Y. Ou; M. Tsai; K. Liu; and K. Chang, "Compressive Behavior of Steel-Fiber-Reinforced Concrete with a High Reinforcing Index", *Journal of Materials in Civil Engineering* © ASCE / February 2012 / 207 - 215
19. Jun - Mo Yang; K. Min; Hyun - Oh Shin; Young - Soo Yoon, "Effect of steel and synthetic fibers on flexural behavior of high-strength concrete beams reinforced with FRP bars", *Composites: Part B* 43(3) (2012) 1077-1086
20. Won K. Lee; Daniel C. Jansen; Kenneth B. Berlin; Ian E. Cohen, "Flexural Cracks in Fiber – Reinforced Concrete Beams with Fiber – Reinforced Polymer Reinforcing Bars", *ACI Structural Journal* V. 107, No. 3, May-June 2010
21. Carreira, D. J. and Chu, K. H. (1985). "Stress-strain relationship for plain concrete in compression." *ACI Journal*, 82(6), 797-804
22. ACI Committee 440.1R-15. Guide for the design and structural of concrete reinforced with Fiber-reinforced polymer (FRP) bars. Farmington Hills(MI): American Concrete Institute, 2015 pp. 83
23. Monika K.; Renata K.; J. Barros; H. Baghi, "Shear behavior of concrete beams reinforced exclusively with longitudinal glass fiber reinforced polymer bars: Experimental research", *Structural concrete* (2018); 19:152-161
24. Shamim A. Sheikh; Zahra Kharal, "Replacement of steel with GFRP for sustainable reinforced concrete", *Constructions and Building Materials* 160 (2018) 767-774
25. Doo-Yeol Yoo; N. Banthia; Young-Soo Yoon, "Predicting service deflection of ultra-high-performance fiber-reinforced concrete beams reinforced with GFRP bars", *Composites Part (B)* 99 (2016) 381-397

26. Doo-Yeol Yoo; N. Banthia; Young-Soo Yoon, “Flexural behavior of ultra-high-performance fiber-reinforced concrete beams reinforced with GFRP and steel rebars”, *Engineering Structures* 111 (2016) 246-262